Article

Immunity

Interleukin-10 receptor signaling promotes the maintenance of a PD-1^{int} TCF-1^{+} CD8^{+} T cell population that sustains anti-tumor immunity

Graphical abstract

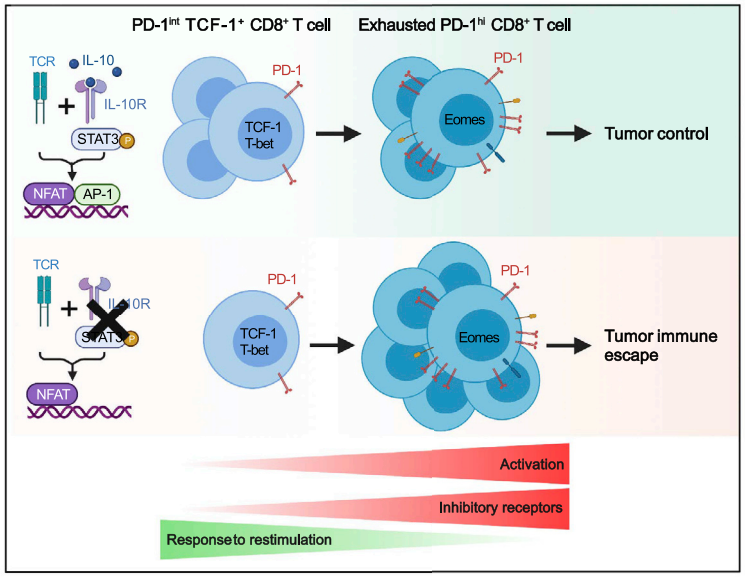

Highlights

- Heterogeneous PD-1 expression identifies CD8^{+} T cells with distinct functions in CLL
- IL-10 prevents activation-induced exhaustion of CD8^{+} T cells and reduces CLL development
- By altering chromatin in CD8^{+} T cells, IL-10R blockade disrupts NFAT:AP-1 cooperativity
- IL-10R loss correlates with T cell exhaustion and poor survival of cancer patients

Authors

Bola S. Hanna, Laura Llaó-Cid, Murat Iskar, ..., Peter Lichter, Marc Zapatka, Martina Seiffert

Correspondence

bola.hanna@hms.harvard.edu (B.S.H.), m.seiffert@dkfz.de (M.S.)

In brief

T cell exhaustion limits anti-tumor immunity and responses to immunotherapy. Using a model of chronic lymphocytic leukemia, Hanna, Llaó-Cid, et al. reveal that the balance between PD-1^{hi}, exhausted CD8^{+} T cells and functional PD-1^{int} CD8^{+} T cells that are associated with tumor progression or tumor control, respectively, is regulated by cell-intrinsic IL-10R signaling.

Hanna et al., 2021, Immunity *54*, 1–17
December 14, 2021
https://doi.org/10.1016/j.immuni.2021.11.004

CellPress

Please cite this article in press as: Hanna et al., Interleukin-10 receptor signaling promotes the maintenance of a PD-1^{int} TCF-1^{+} CD8^{+} T cell population that sustains anti-tumor immunity, Immunity (2021), https://doi.org/10.1016/j.immuni.2021.11.004

Immunity

CellPress

Article

Interleukin-10 receptor signaling promotes the maintenance of a PD-1^{int} TCF-1^{+} CD8^{+} T cell population that sustains anti-tumor immunity

Bola S. Hanna,[1,11,12,*] Laura Llaó-Cid,[1,2,11] Murat Iskar,[1] Philipp M. Roessner,[1] Lara C. Klett,[3] John K.L. Wong,[1] Yashna Paul,[1] Nikolaos Ioannou,[4] Selcen Öztürk,[1] Norman Mack,[1] Verena Kalter,[1] Dolors Colomer,[5] Elías Campo,[5] Johannes Bloehdorn,[6] Stephan Stilgenbauer,[6] Sascha Dietrich,[7] Manfred Schmidt,[8] Richard Gabriel,[8] Karsten Rippe,[3] Markus Feuerer,[9,10] Alan G. Ramsay,[4] Peter Lichter,[1] Marc Zapatka,[1] and Martina Seiffert[1,13,*]

[1]Molecular Genetics, German Cancer Research Center (DKFZ), 69120 Heidelberg, Germany
[2]Faculty of Biosciences, University of Heidelberg, Heidelberg, Germany
[3]Chromatin Networks, German Cancer Research Center (DKFZ), 69120 Heidelberg, Germany
[4]School of Cancer and Pharmaceutical Sciences, Faculty of Life Sciences & Medicine, King's College London, London, UK
[5]Institut d'Investigacions Biomèdiques August Pi i Sunyer (IDIBAPS), Hematopathology Unit, Pathology Department, Hospital Clinic, CIBERONC, University of Barcelona, 08036 Barcelona, Spain
[6]Internal Medicine III, University of Ulm, 89081 Ulm, Germany
[7]Medicine V, University Hospital Heidelberg, 69120 Heidelberg, Germany
[8]Translational Oncology, National Center for Tumor Diseases and German Cancer Research Center, 69120 Heidelberg, Germany
[9]Immune Tolerance, Tumor Immunology Program, German Cancer Research Center (DKFZ), 69120 Heidelberg, Germany
[10]Chair for Immunology, Regensburg Center for Interventional Immunology (RCI), University of Regensburg, 93053 Regensburg, Germany
[11]These authors contributed equally
[12]Present address: Department of Immunology, Harvard Medical School, Boston, MA 02115, USA
[13]Lead contact
*Correspondence: bola.hanna@hms.harvard.edu (B.S.H.), m.seiffert@dkfz.de (M.S.)
https://doi.org/10.1016/j.immuni.2021.11.004

SUMMARY

T cell exhaustion limits anti-tumor immunity and responses to immunotherapy. Here, we explored the microenvironmental signals regulating T cell exhaustion using a model of chronic lymphocytic leukemia (CLL). Single-cell analyses identified a subset of PD-1^{hi}, functionally impaired CD8^{+} T cells that accumulated in secondary lymphoid organs during disease progression and a functionally competent PD-1^{int} subset. Frequencies of PD-1^{int} TCF-1^{+} CD8^{+} T cells decreased upon *Il10rb* or *Stat3* deletion, leading to accumulation of PD-1^{hi} cells and accelerated tumor progression. Mechanistically, inhibition of IL-10R signaling altered chromatin accessibility and disrupted cooperativity between the transcription factors NFAT and AP-1, promoting a distinct NFAT-associated program. Low *IL10* expression or loss of IL-10R-STAT3 signaling correlated with increased frequencies of exhausted CD8^{+} T cells and poor survival in CLL and in breast cancer patients. Thus, balance between PD-1^{hi}, exhausted CD8^{+} T cells and functional PD-1^{int} TCF-1^{+} CD8^{+} T cells is regulated by cell-intrinsic IL-10R signaling, with implications for immunotherapy.

INTRODUCTION

Immune checkpoint blockade by targeting the receptor-programmed death protein 1 (PD-1) and its ligand PD-L1 is an effective strategy for the treatment of multiple tumor entities (Hamid et al., 2013; Topalian et al., 2015; Topalian et al., 2012). Increased expression of PD-1 and other inhibitory receptors including LAG3, CD244, and TIM-3 on CD8^{+} T cells is one of the hallmarks of exhaustion, a differentiation program in CD8^{+} T cells initially described in the course of chronic viral infection (Wherry et al., 2007). T cell exhaustion is characterized by the progressive loss of cytokine production and cytotoxic abilities of T cells (Wherry, 2011; Wherry et al., 2007). Analogous to chronic viral infections, persistent antigenic stimulation also drives tumor-specific T cells to this dysfunctional state (Jiang et al., 2015; Pauken and Wherry, 2015). There is considerable heterogeneity within the exhausted CD8^{+} T cell population in chronic infections, including a progenitor or memory-like cell pool that gives rise to terminally exhausted cells. These precursor cells are defined by intermediate PD-1 expression (PD-1^{int}) and expression of the transcription factor (TF) TCF-1 (encoded by *Tcf7*). This T cell subset confers response to immune checkpoint blockade (Blackburn et al., 2008; Im et al., 2016; Paley et al., 2012; Utzschneider et al., 2016).

In vitro and *in vivo* data imply that the maintenance or loss of function of chronically activated CD8^{+} T cells is highly dependent

Please cite this article in press as: Hanna et al., Interleukin-10 receptor signaling promotes the maintenance of a PD-1^{int} TCF-1^{+} CD8^{+} T cell population that sustains anti-tumor immunity, Immunity (2021), https://doi.org/10.1016/j.immuni.2021.11.004

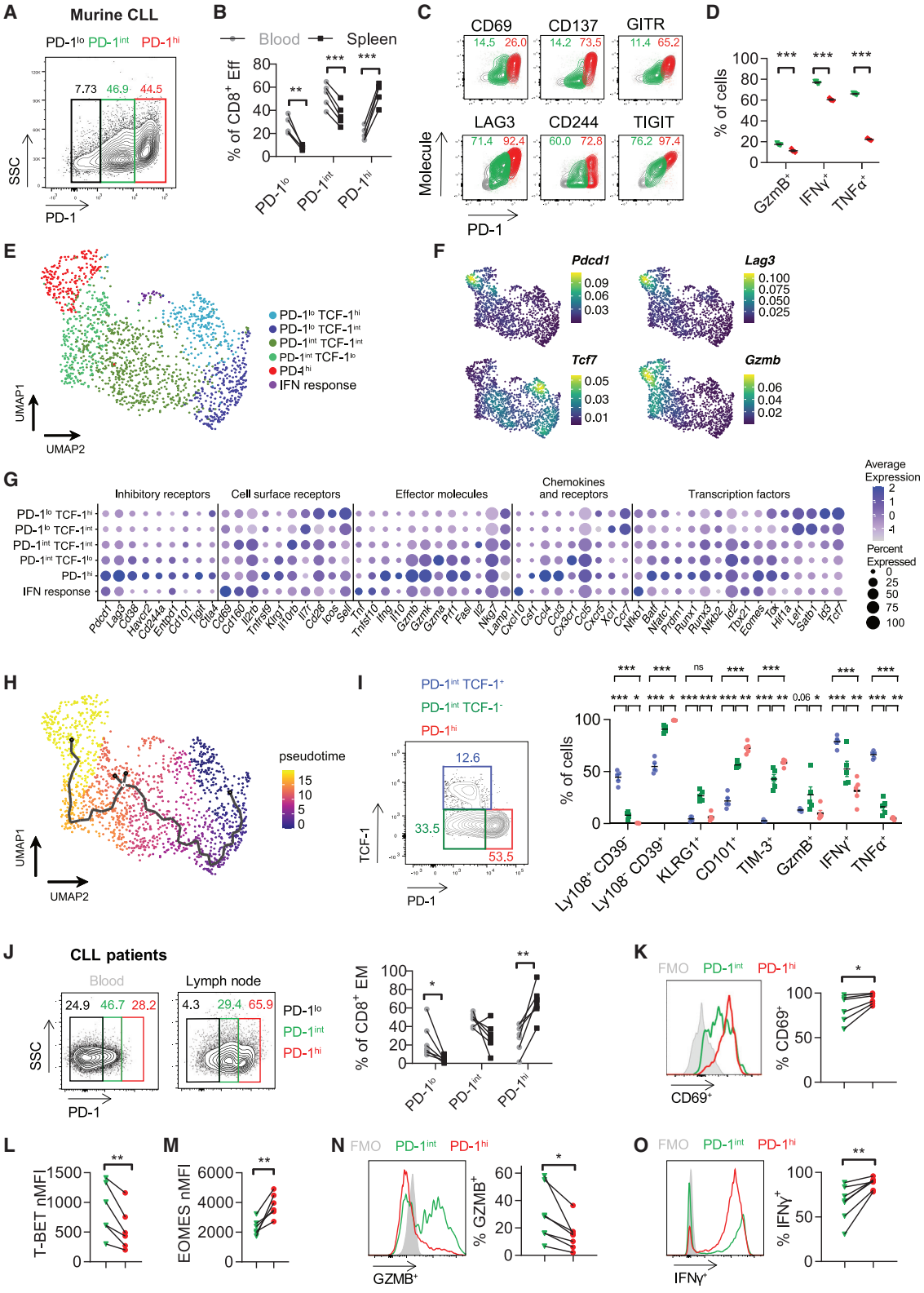

Figure 1. CD8^{+} T cells in human and murine CLL exhibit heterogeneous PD-1 expression associated with distinct functional capacities

(A) Splenic CD8^{+} effector T cells (defined as CD127^{lo} CD44^{int-hi}) from TCL1 AT mice were classified into PD-1^{lo}, PD-1^{int}, and PD-1^{hi} subsets. Representative contour plot is depicted.

(B) Relative abundance of PD-1^{lo}, PD-1^{int}, and PD-1^{hi} subsets in paired blood and spleen samples of TCL1 AT mice (n = 5).

(legend continued on next page)

Please cite this article in press as: Hanna et al., Interleukin-10 receptor signaling promotes the maintenance of a PD-1^{int} TCF-1^{+} CD8^{+} T cell population that sustains anti-tumor immunity, Immunity (2021), https://doi.org/10.1016/j.immuni.2021.11.004

on the cellular microenvironment and the associated cytokine signals. Of particular interest is the role of interleukin-10 (IL-10) in this context. IL-10 is a potent regulatory cytokine that is indispensable for maintenance of self-tolerance and limiting tissue damage during inflammation (Moore et al., 2001; O'Garra and Vieira, 2007). In chronic viral infections, IL-10 impedes viral clearance and promotes persistence of infection (Brooks et al., 2006; Ejrnaes et al., 2006; Parish et al., 2014). The impact of IL-10 in anti-tumor immunity is not clear. IL-10 can impair anti-tumor activity and promote T cell exhaustion in mammary carcinoma and B-16 melanoma models, respectively (Ruffell et al., 2014; Sawant et al., 2019). However, IL-10 or IL-10 receptor (IL-10R) deficiency are associated with poor immune surveillance and increased tumor incidence in skin squamous carcinoma and lymphoma patients (Mumm et al., 2011; Neven et al., 2013). Moreover, IL-10 supplementation leads to an enhanced systemic immune activation and CD8^{+} T cell invigoration in patients with advanced solid tumors (Naing et al., 2018; Qiao et al., 2019). The reason for the divergent reports about the influence of IL-10 on anti-tumor immunity in different settings remains elusive. Because IL-10R is widely expressed by multiple immune cells, IL-10 can impact various cell types, such as antigen-presenting cells and CD8^{+} T cells, plausibly resulting in different immune outcomes at different concentrations. High concentrations of IL-10 delivered therapeutically can directly stimulate CD8^{+} T cell cytotoxicity and proliferation, in contrast to the immunosuppressive nature of IL-10 at low concentrations (Blazar et al., 1998; Emmerich et al., 2012; Groux et al., 1998). Yet, the direct impact of endogenous concentrations of IL-10 on CD8^{+} T cell exhaustion in tumors is not fully clear.

Here we examined this phenomenon using chronic lymphocytic leukemia (CLL), a malignancy of mature CD5^{+} B cells that is characterized by high IL-10 expression (DiLillo et al., 2013; Hanna et al., 2016; Zenz et al., 2010). CD8^{+} T cells in CLL comprise an anti-tumor effector population that undergoes exhaustion in a tissue-specific manner; whereas CD8^{+} T cells in peripheral blood (PB) retain functional capacities, their counterparts in secondary lymphoid organs show increased PD-1 expression and impaired function (Hanna et al., 2019). In the present study, we analyzed the T cell compartment in different tissue sites of CLL patients and the Eμ-TCL1 mouse model of CLL. We identified two distinct populations of PD-1^{+} CD8^{+} T cells: one exhausted and the other functional. IL-10R-STAT3 signaling controlled the balance between these subtypes by limiting excessive activation of CD8^{+} T cells and the transition toward the dysfunctional PD-1^{hi} state with deregulated T cell receptor (TCR) signaling and an aberrant chromatin landscape. These results have implications for our understating of T cell exhaustion in tumors and the design of T cell-based cancer immunotherapies.

RESULTS

CD8^{+} T cells in human and murine CLL exhibit heterogeneous PD-1 expression associated with distinct functional capacities

Adoptive transfer of malignant B cells of Eμ-TCL1 mice (TCL1 AT) into syngeneic wild-type (WT) mice leads to the rapid development of a CLL-like malignancy of mature B cells (Bichi et al., 2002; Hanna et al., 2016; Hofbauer et al., 2011). As seen in patients with CLL, disease development in TCL1 AT mice is associated with the expansion of an oligoclonal CD8^{+} effector T cell population with anti-tumor activity (Hanna et al., 2019). Single-cell RNA-sequencing (scRNA-seq) of splenic CD8^{+} T cells of these mice identified, in addition to naive and memory cell subsets, a clonally expanded effector population with high expression of *Ifng*, *Gzmb*, *Gzmk*, and *Prf1* (Figures S1A–S1D). Expression of *Pdcd1* (encoding PD-1) was exclusive to these effector cells, indicating that PD-1 expression faithfully marked oligoclonal CD8^{+} effector T cells. Using flow cytometry, we confirmed the protein expression of PD-1 on CD8^{+} effector T cells defined by low CD127 expression and intermediate to high CD44 expression (Figure S1E) (Hanna et al., 2019). We identified two distinct effector cell subsets with either intermediate (PD-1^{int}) or high (PD-1^{hi}) PD-1 expression (Figure 1A). The minor low PD-1 expression (PD-1^{lo}) population exhibited a marker profile more similar to memory than effector cells (Figure S1F), and therefore, we did not focus on this population in our further analyses. We detected a higher proportion of the PD-1^{hi} subset in the spleen compared to PB, which was mainly composed of PD-1^{int} cells (Figure 1B). Phenotypic analyses showed that PD-1^{hi} cells had higher expression of activation markers and costimulatory molecules like CD69, CD137 (4-1BB), and GITR (Figures 1C and S1G). Moreover, they showed stronger expression of exhaustion markers like LAG3, CD244, and TIGIT (Figures 1C and S1H), which are induced in chronically activated T cells (Wherry et al., 2007). We further observed differences in the expression of two key TFs that regulate long-term maintenance

(C) Representative contour plots of the expression of CD69, CD137, GITR, LAG3, CD244, and TIGIT in PD-1^{int} (green) and PD-1^{hi} (red) subsets. Numbers depict percentages of positive cells.
(D) Percentage of GzmB^{+}, IFNγ^{+}, and TNFα^{+} cells in PD-1^{int} (green) and PD-1^{hi} (red) CD8^{+} effector T cells (n = 4) from TCL1 AT mice after *ex vivo* stimulation.
(E–H) Single-cell RNA-seq was performed on PD-1^{+} CD8^{+} T cells from a TCL1 AT mouse. (E) UMAP plot showing 6 clusters of PD-1^{+} CD8^{+} T cells. (F) UMAP density plot of the expression of *Pdcd1*, *Lag3, Tcf7*, and *Gzmb*. (G) Dot plot of the expression of inhibitory receptors, cell surface receptors, effector molecules, chemokines and receptors, and transcription factors in the 6 different clusters. (H) Pseudotime trajectory across the 6 clusters of PD-1^{+} CD8^{+} T cells.
(I) Representative contour plot of the expression of TCF-1 in PD-1^{int} and PD-1^{hi} CD8^{+} effector T cells (left panel) and frequency of Ly108^{+} CD39^{-}, Ly108^{-} CD39^{+}, KLRG1^{+}, CD101^{+}, TIM-3^{+}, GzmB^{+}, IFNγ^{+}, and TNFα^{+} cells out of PD-1^{int} TCF-1^{+}, PD-1^{int} TCF-1^{-}, and PD-1^{hi} CD8^{+} effector T cells (right panel).
(J) Paired blood and lymph node samples of CLL patients were analyzed for relative abundance of PD-1^{lo}, PD-1^{int}, and PD-1^{hi} subsets within CD45RO^{+} CCR7^{-} CD8^{+} effector-memory (EM) T cells (n = 6). Representative contour plots and frequencies of subsets are depicted.
(K–O) PD-1^{int} and PD-1^{hi} subsets within the CD8^{+} EM T cell population in lymph nodes of CLL patients (n = 6) were analyzed for the expression of (K) CD69, (L) T-BET, (M) EOMES, and the production of (N) GZMB, and (O) IFNγ upon *ex vivo* stimulation. Representative histograms and quantification of data are depicted. Each symbol represents an individual mouse or patient, and statistical significance was tested by paired t test in (B), (J), (K), (L), (M), (N), and (O), unpaired t test with Welch approximation in (D), or one-way ANOVA with Tukey's multiple comparison test in (I). *$p < 0.05$, **$p < 0.01$, ***$p < 0.001$. Bars indicate mean ± SEM. SSC, side scatter; FMO, fluorescence minus one; nMFI, normalized median fluorescence intensity; ns, not significant.

Please cite this article in press as: Hanna et al., Interleukin-10 receptor signaling promotes the maintenance of a PD-1^{int} TCF-1^{+} CD8^{+} T cell population that sustains anti-tumor immunity, Immunity (2021), https://doi.org/10.1016/j.immuni.2021.11.004

of a CD8^{+} T cell progenitor population in chronic viral infections (Paley et al., 2012; Quigley et al., 2010; Shin et al., 2009), with a higher expression of T-bet in PD-1^{int} compared to PD-1^{hi} cells (Figure S1I) and a vice versa expression pattern of Eomesodermin (Eomes) (Figure S1I). We then tested the functional capacity of the two PD-1^{+} CD8^{+} T cell subsets in response to *ex vivo* restimulation with phorbol myristate acetate (PMA) and ionomycin. PD-1^{int} cells had superior degranulation capacity in this setting, as measured by CD107a presentation on the cell surface (Figure S1J), and produced more GzmB than PD-1^{hi} cells (Figures 1D and S1K). Moreover, PD-1^{int} cells produced more IFNγ and TNFα upon restimulation than PD-1^{hi} cells (Figures 1D and S1K). Yet, no consistent differences in proliferation were detected between the two subsets as measured by Ki-67 staining (Figure S1L).

To assess the validity of using PD-1 expression for defining functionally distinct CD8^{+} effector subsets, we sorted PD-1^{int} and PD-1^{hi} CD8^{+} T cells, as well as naive and memory CD8^{+} T cells, from the spleens of TCL1 AT mice and performed bulk gene expression profiling (GEP) and sequencing of the TCR-beta chain (Figure S2A for sorting strategy). First, we confirmed that PD-1^{int} and PD-1^{hi} effector cells were both clonally expanded T cell populations with a low Shannon diversity index of TCR clonotypes, in contrast to the polyclonal naive and memory T cells (Figures S2B and S2C). Second, unsupervised clustering and principal component analysis (PCA) of GEP data identified the four T cell populations as being distinct, with PD-1^{int} and PD-1^{hi} cells showing greater similarity to each other as compared to naive and memory cells (Figures S2D–S2F). In line with our phenotypic analysis, PD-1^{hi} cells showed high expression of multiple exhaustion marker genes (*Cd244*, *Tigit*, *Lag3*, *Havcr2*, and *Ctla4*) in comparison to PD-1^{int} cells (Figure S2G). Accordingly, gene set enrichment analysis (GSEA) revealed similarities of PD-1^{hi} cells to exhausted CD8^{+} T cells in chronic infections, whereas PD-1^{int} cells resembled memory T cells that develop following acute viral infections (Figures S2H–S2J, Table S1) (West et al., 2011; Wherry et al., 2007). Further, PD-1^{int} cells showed a higher transcript expression of key memory T cell TFs such as *Tcf7*, *Lef1*, and *Bcl6*, and were transcriptionally similar to TCF-1^{+} memory-like CD8^{+} T cells, which sustain the immune response during chronic viral infections (Figures S2G and S2K) (Utzschneider et al., 2016). Finally, our GEP data was highly accordant with data of intratumoral PD-1^{int} and PD-1^{hi} CD8^{+} T cells from patients with non-small cell lung cancer (Figure S2L) (Thommen et al., 2018).

To further analyze the distinct nature of different effector cell subsets, we sorted PD-1^{+} CD8^{+} T cells from a TCL1 AT spleen sample and performed scRNA-seq. We identified six cell clusters that presented with inversely correlated transcript expression of *Pdcd1* and *Tcf7* (Figures 1E and 1F). PD-1^{hi} cells were the most distinct, with the lowest gene expression of *Tcf7* and a strong expression of inhibitory receptors. Inversely, clusters with the lowest *Pdcd1* and highest *Tcf7* expression had a memory-like phenotype with high gene expression of *Sell*, *Ccr7*, and *Lef1*. In addition, we detected two clusters of intermediate *Pdcd1* and low to intermediate *Tcf7* expression. The data further revealed a small cluster of cells that express many IFN response genes. Gene expression of effector molecules was highest in PD-1^{int} TCF-1^{lo} and PD-1^{hi} clusters, with the latter expressing more transcripts of TFs that drive terminal differentiation, such as *Batf*, *Tox*, and *Eomes* (Figure 1G). Pseudotime analysis of our scRNA-seq data further positioned the cell clusters along a trajectory that starts with the two PD-1^{lo} clusters, proceeds via the two PD-1^{int} subsets, and ends with the PD-1^{hi} cluster (Figure 1H), indicating that the PD-1^{int} subsets represent precursor cells of the terminally exhausted PD-1^{hi} cells.

Flow cytometry analyses confirmed that TCF-1 protein expression was restricted to a subset of PD-1^{int} cells while completely absent in the PD-1^{hi} population (Figure 1I). In line with the phenotype of a memory-like precursor population described before (Beltra et al., 2020; Hudson et al., 2019), PD-1^{int} TCF-1^{+} cells were positive for Ly108 (Figures 1I and S2M). Both PD-1^{int} TCF-1^{+} and PD-1^{int} TCF-1^{-} cells showed lower expression of exhaustion markers CD39, CD101, and TIM-3, compared to PD-1^{hi} cells. Functionally, PD-1^{int} TCF-1^{+} cells produced more IFNγ and TNFα, but not GzmB, upon *ex vivo* restimulation than TCF-1^{-} cells (Figure 1I). Yet, PD-1^{int} TCF-1^{-} cells were still proficient in IFNγ and GzmB production, suggesting intact effector function and cytotoxic capacity upon restimulation. Taken together, these data indicate that PD-1^{int} cells comprise both a TCF-1^{+} memory-like precursor subset and TCF-1^{-} cytotoxic effector cells, while PD-1^{hi} cells represent a terminally differentiated, exhausted T cell population with poor response upon restimulation.

We then evaluated whether similar PD-1^{+} T cell subsets were detectable in patients with CLL and focused our analysis on effector-memory T cells, which exhibit the highest expression of PD-1 (Hanna et al., 2019). In line with our data from the TCL1 AT model, we detected an enrichment of PD-1^{hi} cells in disease-affected lymph nodes (LNs) of CLL patients, whereas in PB, PD-1^{int} cells represented the most frequent cell type in most patients (Figure 1J). The PD-1^{hi} population in LNs contained more cells expressing the activation marker CD69 compared to PD-1^{int} counterparts (Figure 1K). Moreover, PD-1^{hi} cells expressed less T-BET and more EOMES (Figures 1L and 1M) and had lower GZMB production compared to PD-1^{int} cells (Figure 1N). PD-1^{hi} cells in LNs from CLL patients comprised a higher percentage of IFNγ^{+} cells compared to PD-1^{int} cells (Figure 1O), indicating that PD-1^{hi} cells in CLL patients retained some functional activity, a feature of exhausted tumor-infiltrating T cells observed in other cancer entities (Li et al., 2019; Miller et al., 2019).

In sum, these data indicate that increased T cell activation in secondary lymphoid organs drives the accumulation of PD-1^{hi}, exhausted T cells in human and murine CLL.

Blocking IL-10 receptor impairs the maintenance of PD-1^{int} TCF-1^{+} CD8^{+} T cells and accelerates CLL progression

We next investigated the signals that regulate the balance between PD-1^{int} and PD-1^{hi} T cell subsets. PD-1^{int} cells expressed more *Ifnar2*, *Il18r1*, and *Il10rb* transcripts compared to PD-1^{hi} cells (Figure S2G), suggesting a potential involvement of inflammatory mediators in modulating the PD-1^{int} cell subset. We focused on IL-10 because CLL development is associated with increased serum concentrations of IL-10 (DiLillo et al., 2013; Hanna et al., 2016). IL-10-GFP reporter mice (Kamanaka et al., 2006) showed induction of IL-10 in multiple cell types in the

Please cite this article in press as: Hanna et al., Interleukin-10 receptor signaling promotes the maintenance of a PD-1^{int} TCF-1^{+} CD8^{+} T cell population that sustains anti-tumor immunity, Immunity (2021), https://doi.org/10.1016/j.immuni.2021.11.004

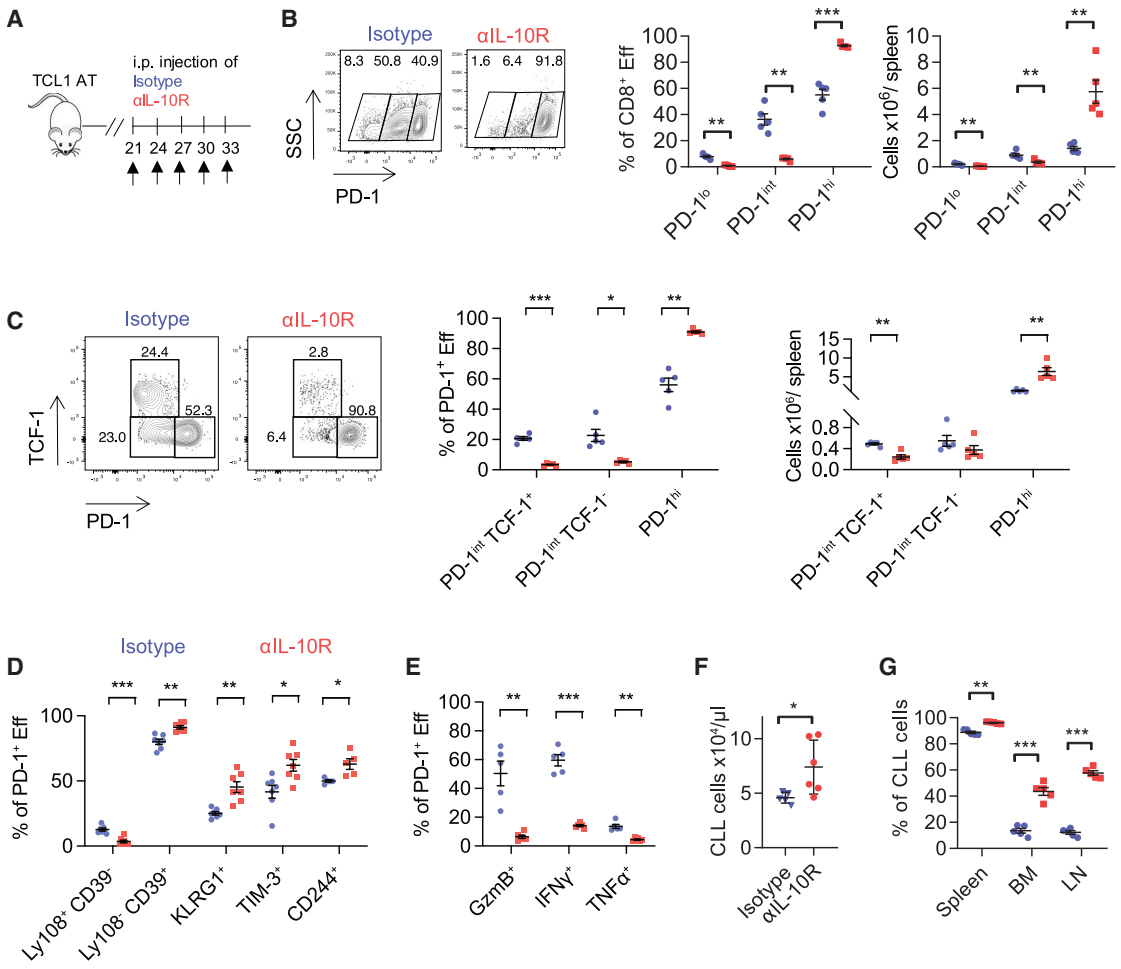

Figure 2. Blocking IL-10 receptor impairs the maintenance of PD-1^{int} TCF-1^{+} CD8^{+} T cells and accelerates CLL progression

(A) Schematic diagram of αIL-10R-blocking antibody treatment in TCL1 AT mice. Analyses of T and CLL cells were performed 15 days after treatment start.

(B) Representative contour plots, relative abundance, and absolute numbers of PD-1^{lo}, PD-1^{int}, and PD-1^{hi} CD8^{+} effector (Eff) T cells in spleen of isotype antibody- and αIL-10R-treated mice.

(C) Representative contour plots, relative abundance, and absolute numbers of PD-1^{int} TCF-1^{+}, PD-1^{int} TCF-1^{-}, and PD-1^{hi} CD8^{+} effector T cells.

(D) Percentage of of Ly108^{+} CD39^{-}, Ly108^{-} CD39^{+}, KLRG1^{+}, TIM-3^{+}, and CD244^{+} cells out of PD-1^{+} CD8^{+} effector T cells.

(E) Percentage of GzmB^{+}, IFNγ^{+}, and TNFα^{+} PD-1^{+} CD8^{+} effector T cells upon *ex vivo* stimulation.

(F–G) (F) Absolute number of CD19^{+} CD5^{+} CLL cells in blood and (G) percentage of CLL cells in spleen, BM, and LN of isotype antibody- and αIL-10R-treated mice. Results are representative of 2 independent experiments. Each symbol represents an individual mouse, and statistical significance was tested by unpaired t test with Welch approximation. *$p < 0.05$, **$p < 0.01$, ***$p < 0.001$. Bars indicate mean ± SEM. FMO, fluorescence minus one.

CLL microenvironment upon TCL1 AT (Figures S3A–S3C). IL-10 was primarily produced by CD4^{+} T cells (both Foxp3^{-} and Foxp3^{+} populations) and CD8^{+} effector T cells and to a lower extent produced by conventional dendritic cells and Ly6C^{lo} monocytes (Figures S3B and S3C). In addition to the increased IL-10 expression in non-malignant cells in the microenvironment, CD5^{+} CD19^{+} CLL cells produced IL-10 when stimulated *ex vivo* with PMA and ionomycin (Figure S3D), highlighting the multiple sources and abundance of this cytokine in CLL.

To assess the role of IL-10 in regulating CD8^{+} T cells in CLL, we treated CLL-bearing mice with IL-10R-blocking antibodies for 15 days to inhibit IL-10-mediated signaling (Figure 2A). The CD8^{+} effector population in the anti(α)-IL-10R-treated mice was almost exclusively composed of PD-1^{hi} cells, with a 4.1-fold higher number of PD-1^{hi} cells in αIL-10R-treated versus control mice (Figure 2B). Accordingly, there were decreased numbers of PD-1^{int} cells; 0.4-fold less PD-1^{int} cells in αIL-10R-treated versus control mice. Within the PD-1^{int} subset, there were less PD-1^{int} TCF-1^{+} compared to TCF-1^{-} cells, resulting in reduced numbers of this progenitor population in comparison to control animals (Figure 2C). Concomitantly, IL-10R blockade induced aggravated features of exhaustion and terminal differentiation in CD8^{+} PD-1^{+} effector T cells, as is evident from the higher expression of the inhibitory receptors CD39, TIM-3, and CD244, and decreased abundance of the Ly108^{+} memory-like progenitor population (Figure 2D).

Functionally, CD8^{+} effector T cells from the αIL-10R group exhibited lower capacity for degranulation (Figure S3E) and production of GzmB and cytokines (IFNγ and TNFα) in response to PMA and ionomycin stimulation (Figures 2E and

Please cite this article in press as: Hanna et al., Interleukin-10 receptor signaling promotes the maintenance of a PD-1^{int} TCF-1^{+} CD8^{+} T cell population that sustains anti-tumor immunity, Immunity (2021), https://doi.org/10.1016/j.immuni.2021.11.004

S3F). The phenotypic and functional changes in CD8^{+} T cells after IL-10R blockade were primarily attributed to their shift toward PD-1^{hi} cells. Nonetheless, lower functional activity was also observed when focusing the analysis on PD-1^{int} or PD-1^{hi} cells from αIL-10R-treated and control mice (Figures S3G and S3H). In line with the general reduction in T cell function upon IL-10R blockade, we detected higher CLL load in PB, spleen, bone marrow (BM), and LNs in αIL-10R-treated mice in comparison to isotype antibody controls (Figures 2F and 2G), indicating a role of IL-10 in controlling CLL progression. Collectively, these data suggest an important role of IL-10R signaling in restraining T cell exhaustion by inhibiting the accumulation of PD-1^{hi} cells and maintaining the PD-1^{int} population that comprises both TCF-1^{+} memory-like precursor cells and TCF-1^{-} functional effector cells possessing intact anti-tumor activity.

Deletion of *Il10rb* or *Stat3* in T cells results in PD-1^{hi} CD8^{+} T cell accumulation and tumor progression

We then sought to evaluate whether the above-mentioned effects were due to intrinsic IL-10R signaling in CD8^{+} T cells and to investigate potential downstream signaling molecules that are involved in IL-10-mediated CD8^{+} T cell responses. We focused on signal transducer and activator of transcription 3 (STAT3), which is rapidly phosphorylated and translocated to the nucleus in response to IL-10 (Finbloom and Winestock, 1995). We transferred CD8^{+} T cells from *Il10rb*$^{+/+}$, *Il10rb*$^{-/-}$, *Stat3*$^{+/+}$, and *Stat3*$^{-/-}$ mice into *Rag2*$^{-/-}$ mice that were subsequently transplanted with malignant B cells from Eμ-TCL1 mice (Figure 3A). As previously described (Hanna et al., 2019), WT CD8^{+} T cells slowed CLL progression in *Rag2*$^{-/-}$ mice as compared to phosphate-buffered saline (PBS)-injected controls (Figure 3B). Unlike transfer of WT CD8^{+} T cells, transfer of *Il10rb*$^{-/-}$ or *Stat3*$^{-/-}$ CD8^{+} T cells resulted in higher tumor load in PB over time and increased spleen and liver weight (Figures 3B, 3C, and S4A). The growth kinetics of leukemic cells in PB and hepato-splenomegaly at the end stage were comparable in mice receiving *Il10rb*$^{-/-}$ or *Stat3*$^{-/-}$ CD8^{+} T cells (Figures 3B, 3C, and S4A). As described before, we observed an increase in total CD8^{+} T cell numbers in PB over time along with leukemia development (Figure S4B) (Hanna et al., 2019), yet only minor differences in CD8^{+} T cell counts in PB and spleen between the four T cell transfer groups (Figures S4B and S4C). Reminiscent of antibody-mediated IL-10R blockade, *Il10rb*$^{-/-}$ and *Stat3*$^{-/-}$ CD8^{+} T cells were mostly PD-1^{hi} cells with 4.2- and 5.9-fold more PD-1^{hi} cells in *Il10rb*$^{-/-}$ and *Stat3*$^{-/-}$ versus control mice, respectively (Figures 3D, S4D, and S4E). Accordingly, decreased numbers of PD-1^{int} CD8^{+} T cells were observed, with 0.4- and 0.7-fold less PD-1^{int} cells in *Il10rb*$^{-/-}$ and *Stat3*$^{-/-}$ versus control mice, respectively. Deletion of *Il10rb* or *Stat3* resulted in lower frequencies of PD-1^{int} TCF-1^{+} CD8^{+} T cells (Figure S4F shows exemplary data of *Stat3*$^{-/-}$ mice). This correlated with higher expression of exhaustion markers (CD244, TIGIT, CD39, CD101, and TIM-3) on *Il10rb*$^{-/-}$ and *Stat3*$^{-/-}$ CD8^{+} T cells compared to respective controls (Figure 3E; Figure S4G shows exemplary data of *Stat3*$^{-/-}$ mice). Finally, CD8^{+} T cells that lack *Il10rb* or *Stat3* showed inferior functional capacity, as is evident from lower GzmB and cytokine production in comparison to T cells from WT mice (Figures 3F and S4H). The increase in exhaustion marker expression and the drop in functional mediators of CD8^{+} T cells were also observed when focusing the analysis on the PD-1^{hi} subset (Figures S4I–S4K).

Dysfunction of T cells in CLL is associated with defective immune synapse formation (Ramsay et al., 2008). We therefore quantified conjugation of tumor-experienced CD8^{+} T cells with CLL cells in co-cultures and observed a lower rate of conjugation and a reduced synapse area of *Il10rb*$^{-/-}$ compared to WT T cells (Figures 3G and 3H). Further, accumulation of GzmB at the synapse of CD8^{+} T cells with CLL cells was impaired in *Il10rb*$^{-/-}$ cells (Figure 3I), confirming the relevance of IL-10R signaling for proper function of CLL-reactive T cells.

To further validate the relevance of IL-10R signaling for anti-tumor activity of T cells, we sorted tumor-experienced WT or *Il10rb*$^{-/-}$ CD8^{+} PD-1^{+} T cells from leukemic TCL1 AT mice and transferred them into naive *Rag2*$^{-/-}$ mice that were subsequently challenged with TCL1 tumor. In line with their signs of dysfunction, mice transplanted with *Il10rb*$^{-/-}$ T cells showed a higher tumor load compared to mice receiving WT T cells (Figure S4L). Altogether, these results demonstrate that IL-10R-STAT3 signaling has an important, cell-intrinsic role in limiting CD8^{+} T cell exhaustion and maintaining immune control of CLL.

Blockade or deletion of IL-10R-STAT3 signaling transiently activates CD8^{+} T cells prior to inducing their exhaustion

Subsequently, we investigated the mechanisms by which IL-10 controls the anti-tumoral activity of CD8^{+} T cells in CLL. The impaired T cell function after IL-10R blockade could be explained either by the ability of IL-10 to directly stimulate anti-tumoral T cells as previously suggested (Mumm et al., 2011), or, conversely, by an immunoregulatory role of IL-10 that protects T cells from activation-induced dysfunction. We deemed the latter possibility more likely because PD-1^{int} cells, a population that is lost after IL-10R blockade, appeared less activated compared to their PD-1^{hi} counterparts (Figure 1C). In line with this hypothesis, we observed a higher frequency of CD8^{+} effector T cells expressing activation molecules, such as CD69, CD137, and GITR, in the αIL-10R group (Figure 4A). Similar results were observed in *Il10rb*$^{-/-}$ and *Stat3*$^{-/-}$ CD8^{+} T cells adoptively transferred with TCL1 tumors in *Rag2*$^{-/-}$ mice (Figure 4B). Accordingly, it seemed plausible that initial signs of activation preceded the drop in CD8^{+} T cell function that happened *in vivo* after IL-10R blockade. To test this possibility, we treated CLL-bearing mice with αIL-10R antibodies for 5 or 15 days (Figure 4C). In contrast to mice that received continuous treatment for 15 days, blockade of IL-10R for 5 days had no effect on the frequency of PD-1^{int} and PD-1^{hi} cells (Figure S4M), or the expression of other inhibitory receptors, such as CD244 (Figure S4N). While prolonged IL-10R blockade resulted in a considerable drop in T cell function, short-term αIL-10R treatment conversely induced higher cytokine expression (Figure 4D), indicating that prolonged IL-10R blockade resulted in impairment of T cells following a transient enhancement of their function. In sum, these data demonstrate a crucial role of IL-10 in preserving anti-tumor immune response in CLL by protecting CD8^{+} T cells from transitioning from an activated into a dysfunctional PD-1^{hi} state.

Please cite this article in press as: Hanna et al., Interleukin-10 receptor signaling promotes the maintenance of a PD-1^{int} TCF-1^{+} CD8^{+} T cell population that sustains anti-tumor immunity, Immunity (2021), https://doi.org/10.1016/j.immuni.2021.11.004

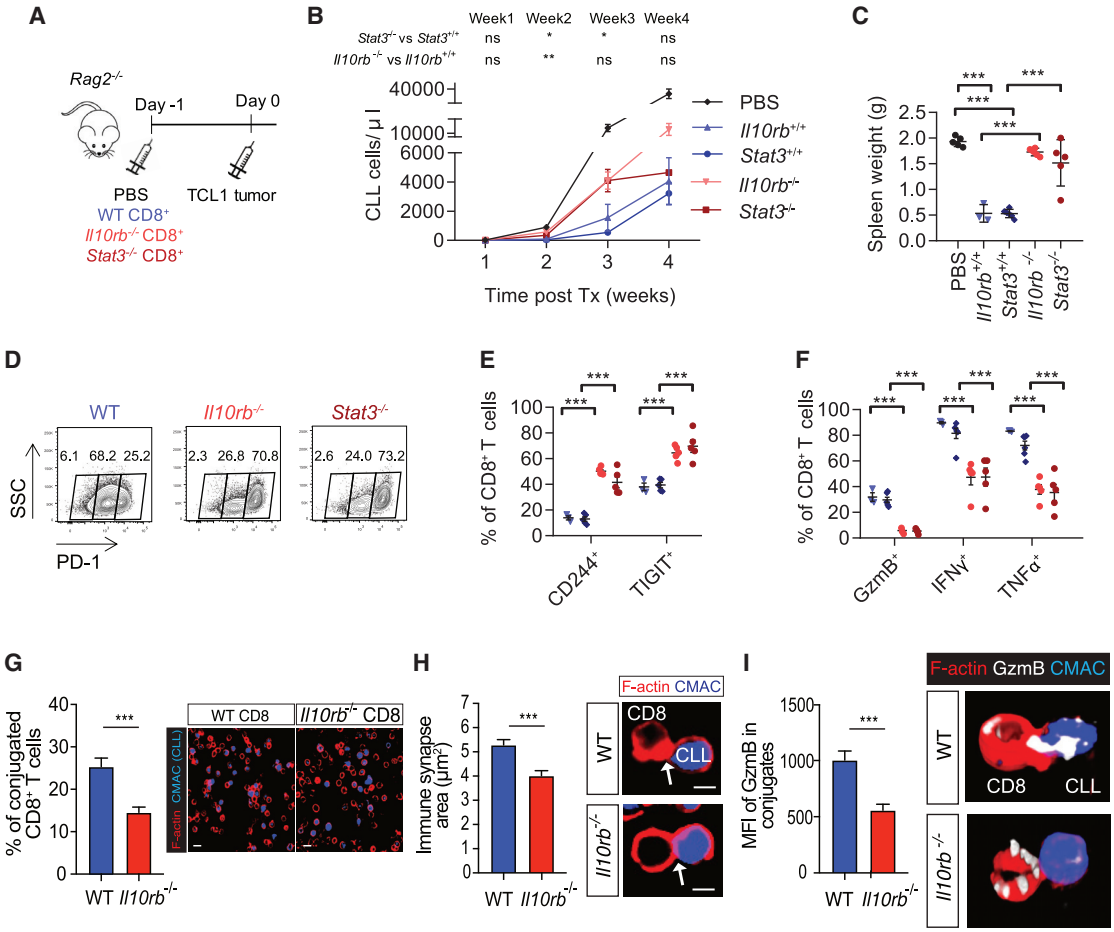

Figure 3. Deletion of *Il10rb* or *Stat3* in T cells results in PD-1^{hi} CD8^{+} T cell accumulation and tumor progression

(A) Schematic diagram of adoptive transfer of CD8^{+} T cells from *Il10rb*$^{-/-}$, *Stat3*$^{-/-}$, or control mice into *Rag2*$^{-/-}$ recipients subsequently transplanted with TCL1 tumor cells.

(B) Absolute numbers of CLL cells in PB over time.

(C) Spleen weight of *Rag2*$^{-/-}$ mice 5 weeks after TCL1 AT.

(D) Representative contour plots showing PD-1^{lo}, PD-1^{int}, and PD-1^{hi} subsets of CD8^{+} T cells.

(E) Percentage of CD8^{+} T cells expressing CD244 and TIGIT.

(F) Percentage of CD8^{+} T cells producing GzmB, IFNγ, and TNFα upon *ex vivo* stimulation.

(G–I) CLL cells and CD8^{+} T cells were isolated from spleen 5 weeks after TCL1 AT. CLL cells were stained with CMAC (blue), mixed with T cells, and immobilized to slides for analysis of intercellular interactions after F-actin and GzmB staining. (G) Quantification of CD8^{+} T cell:CLL cell conjugates (n = 4) and representative images. The original magnification is 63× (scale bars: 10 μm). (H) Quantification of immune synapse formation (F-actin area, μm^2) and representative medial optical sections (scale bars: 5 μm) with arrows indicating immune synapse at T cell contact sites with target CLL cells (n = 4). (I) Mean fluorescence intensity (MFI) of GzmB at all CD8^{+} T cell contact sites with target CLL cells (n = 4) and representative 3D volume-rendered images of GzmB-expressing CD8^{+} T cell conjugates with CLL cells (blue).

Each symbol represents an individual mouse, and statistical significance was tested by one-way ANOVA with Tukey's multiple comparison test in (C), (E), and (F), or unpaired t test in (G), (H), and (I). *p < 0.05, **p < 0.01, ***p < 0.001. Bars indicate mean ± SEM.

Loss of IL-10R-STAT3 signaling impairs CD8^{+} T cell proliferation in tumor-bearing mice

To further elucidate the role of IL-10R signaling in PD-1^{hi} effector T cells, we performed GEP of flow cytometry-sorted PD-1^{hi} CD8^{+} effector T cells from mice treated for 15 days with control antibody or αIL-10R. This analysis showed a lower transcript expression of 81 cell cycle-related genes in αIL-10R-treated mice (Figures 5A and S5A–S5B). Accordingly, GSEA of these data identified DNA replication, mitotic, and cell cycle-related pathways to be less abundant upon αIL-10R treatment (Figures 5B and S5C; Table S1). In line with these results, IL-10R blockade resulted in lower effector T cell proliferation, as measured by Ki-67 staining, which was also evident when focusing the analysis on PD-1^{hi} cells (Figures 5C and S5D). Furthermore, we detected lower percentages of Ki-67^{+} cells in *Il10rb*$^{-/-}$ and *Stat3*$^{-/-}$ CD8^{+} T cells that were isolated from CLL-bearing *Rag2*$^{-/-}$ mice (Figure 5D). Additionally, IL-10 treatment of αCD3/CD28-stimulated CD8^{+} T cells *in vitro* resulted in enhanced cell proliferation, as measured by carboxyfluorescein succinimidyl ester (CFSE) dilution (Figure S5E). Thus, our data link IL-10R signaling with enhanced proliferation of activated CD8^{+}

Please cite this article in press as: Hanna et al., Interleukin-10 receptor signaling promotes the maintenance of a PD-1^{int} TCF-1^{+} CD8^{+} T cell population that sustains anti-tumor immunity, Immunity (2021), https://doi.org/10.1016/j.immuni.2021.11.004

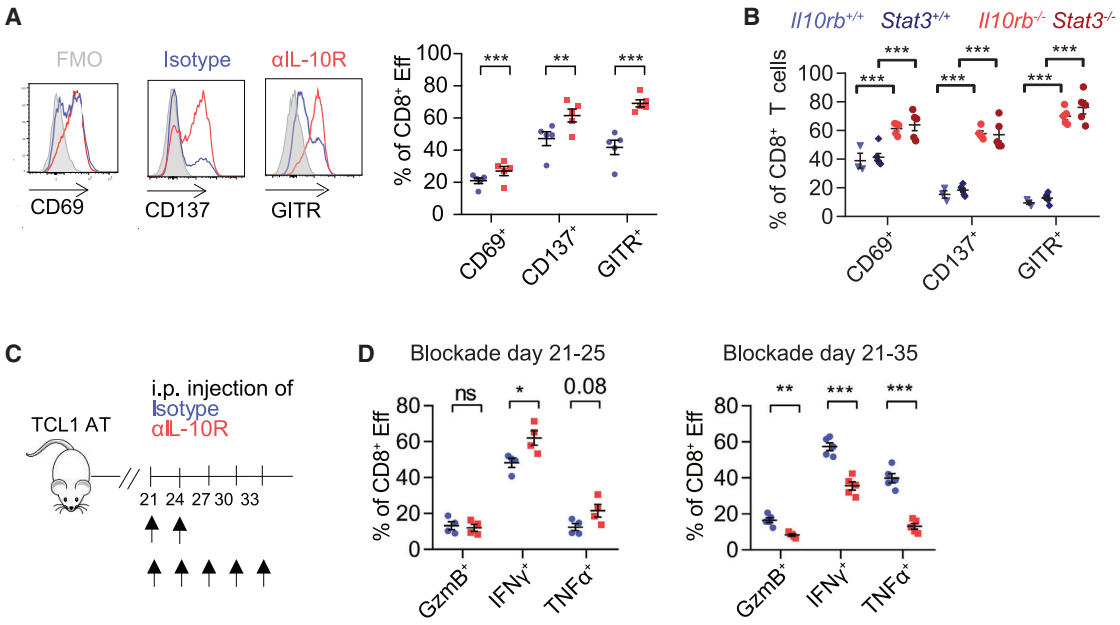

Figure 4. Blockade or deletion of IL-10R-STAT3 signaling transiently activates CD8^{+} T cells prior to inducing their exhaustion

(A) Representative histograms and relative frequency of CD69^{+}, CD137^{+}, and GITR^{+} cells in splenic CD8^{+} effector T cells of TCL1 AT mice treated for 15 days with isotype antibody or αIL-10R (n = 6).

(B) Percentage of CD69^{+}, CD137^{+}, and GITR^{+} cells in splenic CD8^{+} T cells from CLL-bearing *Rag2*$^{-/-}$ mice injected with WT, *Il10rb*$^{-/-}$ or *Stat3*$^{-/-}$ CD8^{+} T cells.

(C) Schematic diagram of short-term (5 days) and long-term (15 days) IL-10R blockade in TCL1 AT mice.

(D) Percentage of GzmB^{+}, IFNγ^{+}, and TNFα^{+} cells in splenic CD8^{+} effector T cells after short-term or long-term IL-10R blockade *in vivo* and upon *ex vivo* stimulation (n = 4–5). Each symbol represents an individual mouse, and statistical significance was tested by unpaired t test with Welch approximation in (A) and (D), or one-way ANOVA with Tukey's multiple comparison test in (B). *p < 0.05, **p < 0.01, ***p < 0.001. Bars indicate mean ± SEM. FMO, fluorescence minus one; ns, not significant.

T cells *in vitro* and *in vivo*, as previously suggested for human CD8^{+} memory T cells (Nizzoli et al., 2016).

To confirm these results, we tested whether the lack of IL-10R signaling confers competitive disadvantage for CD8^{+} T cells in the presence of WT counterparts. We transferred a 1:1 mixture of *Il10rb*$^{-/-}$ and congenically-labeled WT CD8^{+} T cells into *Rag2*$^{-/-}$ mice that were subsequently transplanted with TCL1 tumor cells (Figure 5E). 5 weeks later, we detected an enrichment of WT CD8^{+} T cells and a lower percentage of Ki-67^{+} cells within the *Il10rb*$^{-/-}$ CD8^{+} T cell population (Figures 5F and 5G), confirming the role of IL-10 in maintaining T cell proliferation. This experimental setup also enabled us to simultaneously compare WT and *Il10rb*$^{-/-}$ CD8^{+} T cells in the same recipients and thereby to exclude the possibility that the changes in T cell function and subset distribution in mice transplanted with *Il10rb*$^{-/-}$ or WT CD8^{+} T cells were secondary to differences in tumor load or inflammatory milieu. In agreement with our previous results, *Il10rb*$^{-/-}$ CD8^{+} T cells were enriched in the PD-1^{hi} subset and exhibited considerably lower GzmB and cytokine production in comparison to their co-transferred WT counterparts (Figures 5H and 5I).

IL-10R blockade alters chromatin and reduces DNA accessibility of AP-1 in CD8^{+} T cells

As T cell exhaustion is linked to a state-specific epigenetic landscape (Sen et al., 2016), we explored whether the phenotypic and functional changes in CD8^{+} T cells following IL-10R blockade can be explained by changes in chromatin accessibility. Thus, we performed ATAC-seq analysis of PD-1^{hi} cells from mice treated for 15 days with αIL-10R antibodies and compared them to PD-1^{hi} and PD-1^{int} cells from control mice (the almost complete loss of PD-1^{int} cells in αIL-10R-treated mice hindered their inclusion in this comparison). Unsupervised clustering and PCA showed that PD-1^{hi} cells from αIL-10R mice clustered independently of PD-1^{hi} and PD-1^{int} cells from control mice (Figure 6A). Compared to control PD-1^{hi} cells, αIL-10R PD-1^{hi} cells showed 3,433 and 2,391 open chromatin regions (OCRs) with significantly higher or lower accessibility, respectively (Figure 6B). A comparison of these differential sites to previously published ATAC-seq profiles of effector and exhausted CD8^{+} T cell subsets (Scott-Browne et al., 2016) revealed similarities of αIL-10R cells with exhausted CD8^{+} T cells, but not with functional effector cells (Figure 6C; depleted OCRs in αIL-10R are reduced and enriched OCRs are enhanced in exhausted T cells). The ATAC-seq data further revealed that αIL-10R cells had a pronounced loss of OCRs that are in close proximity to the gene loci of *Tcf7*, *Tbx21*, and *Gzmb* (Figure S6A). These results were in line with the observed reduced protein expression of TCF-1 and GzmB in αIL-10R T cells (Figures 2D, 2E, S3F, and S3I). Next, we used the GREAT enrichment analysis tool to interrogate potential pathways affected by IL-10R blockade in an unbiased manner (McLean et al., 2010). This analysis strongly suggested TCR signaling as the most downregulated

Please cite this article in press as: Hanna et al., Interleukin-10 receptor signaling promotes the maintenance of a PD-1^{int} TCF-1^{+} CD8^{+} T cell population that sustains anti-tumor immunity, Immunity (2021), https://doi.org/10.1016/j.immuni.2021.11.004

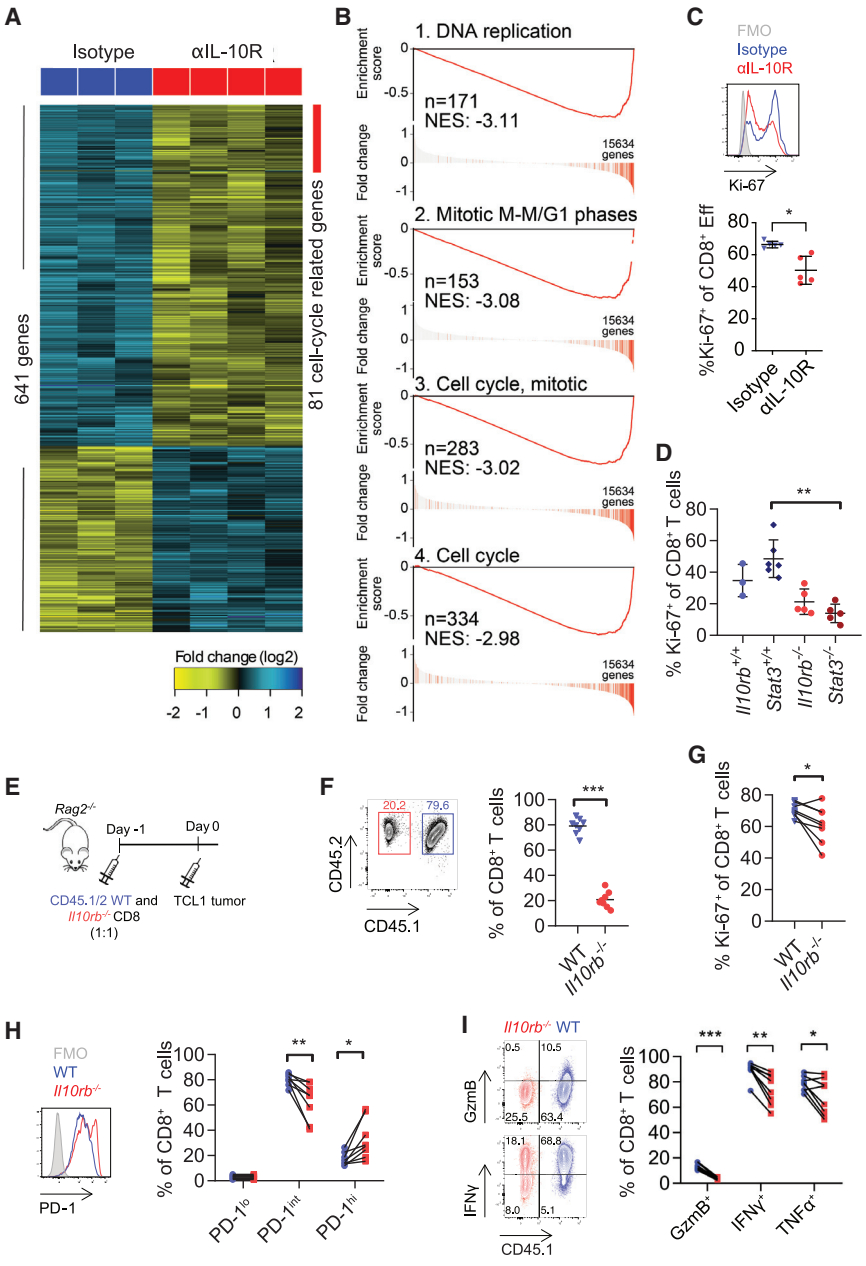

Figure 5. Loss of IL-10R-STAT3 signaling impairs CD8^{+} T cell proliferation in tumor-bearing mice

(A–B) Gene expression profiling (GEP) was performed on PD-1^{hi} CD8^{+} T cells from spleens of CLL-bearing mice treated for 15 days with isotype antibody or αIL-10R (n = 3–4). (A) Heatmap of the top differentially expressed genes with a p value < 0.05 and absolute log2 fold change > 0.5. (B) Top differential pathways between the two treatment groups identified by gene set enrichment analysis (GSEA).

(C) Representative histogram and percentage of Ki-67^{+} cells of CD8^{+} effector T cells in isotype antibody- and αIL-10R-treated mice (n = 5).

(D) Percentage of Ki-67^{+} cells of *Il10rb*$^{-/-}$, *Stat3*$^{-/-}$, or control CD8^{+} T cells (n = 5; experiment shown in Figure 3).

(E) Schematic diagram of adoptive transfer of a 1:1 mixture of CD8^{+} T cells from congenically-labeled WT (CD45.1^{+} CD45.2^{+}) and *Il10rb*$^{-/-}$ (CD45.1^{-} CD45.2^{+}) mice into *Rag2*$^{-/-}$ mice that were subsequently transplanted with TCL1 tumor cells.

(F) Representative contour plot and relative abundance of WT and *Il10rb*$^{-/-}$ cells within CD8^{+} T cells (n = 8).

(G–I) (G) Percentage of Ki-67^{+} CD8^{+} T cells, (H) representative histogram and relative abundance of PD-1^{lo}, PD-1^{int}, and PD-1^{hi} subsets, and (I) representative contour plots and relative abundance of GzmB^{+}, IFNγ^{+}, and TNFα^{+} cells upon *ex vivo* stimulation of WT and *Il10rb*$^{-/-}$ CD8^{+} T cells. Each symbol represents an individual mouse, and statistical significance was tested by unpaired t test with Welch approximation in (C) and (F), one-way ANOVA with Tukey's multiple comparison test in (D), or paired t test in (G), (H), and (I). *p < 0.05, **p < 0.01, ***p < 0.001. Bars indicate mean ± SEM.

pathway in T cells from αIL-10R mice (Figure 6D). Accordingly, key TCR signaling genes, such as *Zap70* and *Lat*, showed a depletion of multiple OCR peaks in αIL-10R PD-1^{hi} cells (Figure 6E and data not shown), indicating that IL-10R blockade results in the dysregulation of TCR signaling. Along this line, *in vitro* data showed that IL-10 treatment of TCR-stimulated CD8^{+} T cells resulted in higher phosphorylation of TCR downstream targets, such as ZAP70 and ERK1/2, compared to control cells (Figures S6B and S6C).

To elucidate potential TFs affected by IL-10R blockade, we performed TF motif analysis using *Homer*. Most of the TFs predicted by this analysis were known downstream targets of TCR signaling (Figure 6F, Table S2). To this end, Nur77 and NFAT were among the most enriched TFs after IL-10R blockade, whereas several AP-1-family TFs such as Batf, Fra1 (Fosl1), and JunB were lost (Figure 6F). Using TF footprint analysis, we further confirmed increased NFATc1 binding in αIL-10R PD-1^{hi} T cells (Figure 6G). Enrichment of NFAT and depletion of AP-1 TFs in T cells of αIL-10R-treated mice suggested that IL-10R blockade induces the loss of NFAT:AP-1 cooperativity, which has been shown to drive T cell exhaustion (Martinez et al., 2015). To corroborate this hypothesis, we compared the differential OCRs of αIL-10R cells to a previously published ATAC-seq profile of a mutant version of NFAT that cannot interact with AP-1 (NFAT:CA-RIT). Transfection of this mutant in CD8^{+} T cells results in a chromatin program that resembles that of exhausted cells (Scott-Browne et al., 2016). We observed a concordance of differential OCRs of αIL-10R cells with those induced in cells transfected with NFAT:CARIT (Figure 6H). To further validate the dysregulation of NFAT:AP-1 activity after IL-10R blockade, we quantified protein expression of c-Jun after PMA and ionomycin stimulation of WT, *Il10rb*$^{-/-}$, and *Stat3*$^{-/-}$ CD8^{+} T cells isolated from

Please cite this article in press as: Hanna et al., Interleukin-10 receptor signaling promotes the maintenance of a PD-1^{int} TCF-1^{+} CD8^{+} T cell population that sustains anti-tumor immunity, Immunity (2021), https://doi.org/10.1016/j.immuni.2021.11.004

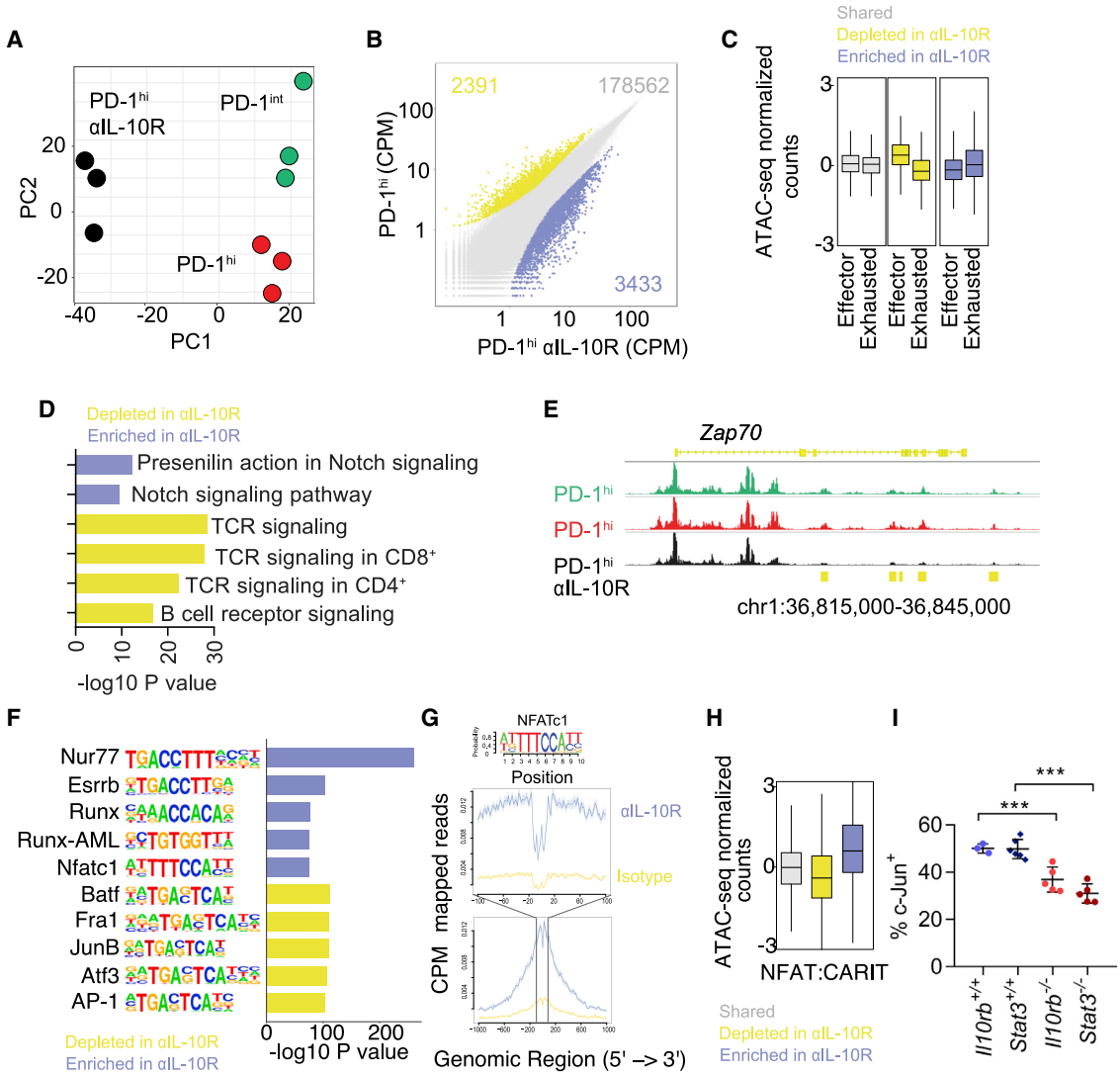

Figure 6. IL-10R blockade alters chromatin and reduces DNA accessibility of AP-1 in CD8^{+} T cells

(A) Principal component analysis (PCA) of ATAC-seq profiles of PD-1^{int} and PD-1^{hi} CD8^{+} T cells from isotype antibody-treated mice, and PD-1^{hi} CD8^{+} T cells from αIL-10R-treated mice (n = 3).

(B) Scatterplots of mean ATAC-seq counts per peak (CPM) comparing PD-1^{hi} CD8^{+} T cells from isotype antibody- and αIL-10R-treated mice.

(C) Boxplots of ATAC-seq counts of effector and exhausted T cells in viral infections (Scott-Browne et al., 2016) at the shared (gray), less (yellow), or more (purple) accessible regions in PD-1^{hi} αIL-10R- versus isotype antibody-treated controls.

(D–G) (D) GREAT pathway analysis of differentially accessible open chromatin regions (OCRs), (E) representative ATAC-seq tracks for *Zap70* locus, (F) enrichment of transcription factor (TF) binding motifs in OCRs gained (purple) or lost (yellow), and (G) TF footprint for NFATc1 in PD-1^{hi} cells in αIL-10R- versus isotype antibody-treated controls.

(H) Boxplots of ATAC-seq counts of CD8^{+} T cells transduced with NFAT-CA-RIT mutant (Scott-Browne et al., 2016) at the shared (gray), less (yellow), or more (purple) accessible regions in PD-1^{hi} αIL-10R- versus isotype antibody-treated controls.

(I) Percentage of c-Jun expression in response to *ex vivo* stimulation in *Il10rb*$^{-/-}$, *Stat3*$^{-/-}$, or control CD8^{+} T cells (n = 5; experiment shown in Figure 3). Each symbol in (I) represents an individual mouse, and statistical significance was tested by one-way ANOVA with Tukey's multiple comparison test. ***p < 0.001. Bars indicate mean ± SEM.

CLL-bearing mice. Accordingly, we observed lower c-Jun expression in *Il10rb*$^{-/-}$ and *Stat3*$^{-/-}$ CD8^{+} T cells compared to WT controls (Figure 6I), reminiscent of the depletion of AP-1 motifs. Altogether, these data show that IL-10R blockade results in chromatin remodeling and dysregulation of NFAT:AP-1 cooperativity, which has been previously linked to CD8^{+} T cell dysfunction (Martinez et al., 2015).

Loss of IL-10R-STAT3 signaling correlates with poor survival and CD8^{+} T cell exhaustion in cancer patients

To validate the relevance of IL-10R-STAT3 signaling in maintaining immune control in cancer patients, we first examined the correlation of *IL10* gene expression with survival in a cohort of CLL patients (n = 73). In contrast to previous studies showing that high IL-10 serum concentrations are predictive for worse

Please cite this article in press as: Hanna et al., Interleukin-10 receptor signaling promotes the maintenance of a PD-1^{int} TCF-1^{+} CD8^{+} T cell population that sustains anti-tumor immunity, Immunity (2021), https://doi.org/10.1016/j.immuni.2021.11.004

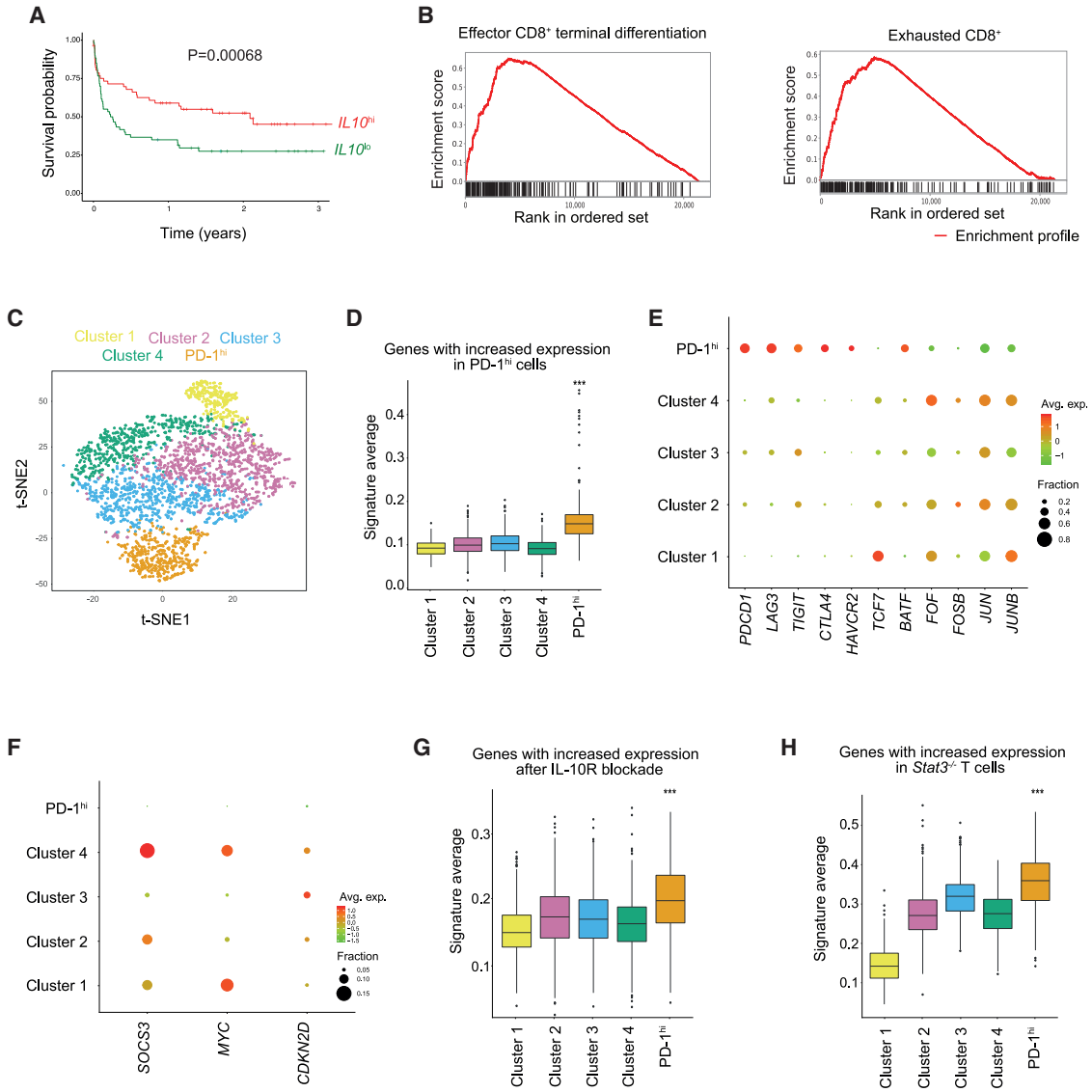

Figure 7. Loss of IL-10R-STAT3 signaling correlates with poor survival and CD8^{+} T cell exhaustion in cancer patients

(A) Time-to-treatment in untreated CLL patients with high or low *IL10* gene expression (n = 73).

(B) GSEA of ranked-list of genes (fold change) from the comparison of IL-10R germline-deficient versus control lymphoma patients (Neven et al., 2013) using signatures of terminally differentiated effector (Sarkar et al., 2008) and exhausted CD8^{+} T cells (Doering et al., 2012).

(C–H) Single-cell RNA-seq analysis of tumor-infiltrating CD8^{+} T cells in breast cancer patient BC9 (Azizi et al., 2018). (C) tSNE plot identifying 5 different CD8^{+} T cell clusters, including one with high expression of PD-1 (orange). (D) Average expression of genes with higher expression in PD-1^{hi} versus PD-1^{int} CD8^{+} T cells in TCL1 AT mice. (E) Dot plot of the expression of exhaustion hallmark genes, TFs, and AP-1 family members. (F) Dot plot of the expression of key STAT3 target genes. (G) Average expression of genes with higher expression in PD-1^{hi} CD8^{+} T cells from TCL1 AT mice upon αIL-10R blockade, and (H) Average expression of genes with higher expression in *Stat3*$^{-/-}$ versus WT follicular helper T cells (Ray et al., 2014). Statistical significance in (D), (G), and (H) was calculated using a Kruskal-Wallis test. ***p < 0.001. tSNE, t-distributed stochastic neighbor embedding; Avg. exp., average expression.

outcomes in CLL (Fayad et al., 2001), high *IL10* transcript expression correlated with longer time-to-treatment in a cohort of untreated CLL patients (Figure 7A). This was further confirmed in an independent cohort of untreated CLL patients where *IL10* transcript expression was independent of the tumor load, and higher *IL10* expression correlated with longer progression-free and overall survival independently of the *IGHV* mutational status, a strong prognostic marker in CLL, in these samples (Figures S7A–S7C). We then compared GEP data of lymphoma patients harboring germline genetic deficiencies in IL-10R (Neven et al., 2013). In comparison to IL-10R-proficient lymphoma cases, these tumors were enriched in gene signatures of terminally differentiated and exhausted CD8^{+} T cells (Figure 7B). To evaluate the relevance of IL-10R-STAT3 signaling in CD8^{+} T cells in other human cancers, we utilized published scRNA-seq data of tumor-infiltrating T cells from three breast cancer patients (Azizi et al., 2018). Using t-distributed stochastic neighbor embedding (tSNE) dimensionality reduction of these data, we identified a

Please cite this article in press as: Hanna et al., Interleukin-10 receptor signaling promotes the maintenance of a PD-1^{int} TCF-1^{+} CD8^{+} T cell population that sustains anti-tumor immunity, Immunity (2021), https://doi.org/10.1016/j.immuni.2021.11.004

PD-1^{hi} cell cluster representing 6%–16% of CD8^{+} T cells in each patient. These cells showed a specific enrichment in PD-1^{hi} CD8^{+} T cell signature genes and presented with high expression of transcripts encoding exhaustion hallmark genes such as *PDCD1*, *LAG3*, *CTLA4*, *TIGIT*, and *HAVCR2* (Figures 7C–7E and S7D–E). The PD-1^{hi} cluster further expressed lower transcripts of *TCF7* compared to the other four cell clusters (Figures 7E and S7F). In line with our data from TCL1 AT mice, several AP-1 family TF genes, such as *FOS*, *FOSB*, *JUN*, and *JUNB*, were considerably less abundant in the PD-1^{hi} cluster (Figures 7E and S7F), and key IL-10R-STAT3 target genes, like *SOCS3*, *MYC*, and *CDKN2D,* showed lower transcript expression in this cluster as well (Figures 7F and S7G). The PD-1^{hi} cluster was enriched for genes we identified to be upregulated in CD8^{+} T cells in response to IL-10R blockade in leukemic TCL1 AT mice (Figures 7G and S7H). Moreover, the gene signature of this PD-1^{hi} cell cluster showed high concordance with a previously published gene signature of STAT3-deficient follicular helper T cells (Figures 7H and S7I) (Ray et al., 2014). Altogether, these data confirm the relevance of IL-10R-STAT3 signaling in preventing CD8^{+} T cell exhaustion and terminal differentiation in cancer patients.

DISCUSSION

Understanding the heterogeneity of T cells in tumors is crucial for the design of successful immunotherapies, as the exhaustion state of T cells determines their potential for reinvigoration (McLane et al., 2019). Recent studies in chronic viral infection and cancer identify distinct exhausted T cell subsets and suggest a hierarchical scheme in which the TFs TCF-1, T-BET, and TOX coordinate their development and dynamics (Beltra et al., 2020; Chen et al., 2019; Hudson et al., 2019). Prolonged TCR engagement is the main inducer of a dysfunctional PD-1^{hi} CD8^{+} T cell subset, which shows features of terminal differentiation in chronic infection models (Man et al., 2017). Similarly, T cell dysfunction is also described in cancer as a dynamic, antigen-driven process (Schietinger et al., 2016). The functionally distinct PD-1^{hi} and PD-1^{int} TCF1^{+} CD8^{+} T cell subsets we identified in CLL are highly similar to respective cell subsets in solid tumors. Thus, the mechanistic insights we gain here are likely of relevance for immune escape in cancer in general.

IL-10 mediates T cell exhaustion in chronic viral infections (Brooks et al., 2006; Ejrnaes et al., 2006; Parish et al., 2014). But IL-10 also enhances the activity of tumor-resident CD8^{+} T cells and their effective control of tumor growth in several tumor mouse models (Emmerich et al., 2012; Guo et al., 2021). Given our current results, the contradicting effects of IL-10 in different disease models can be explained by its divergent impact on different stages of T cell activation. Snell et al. (2018) show that the outcome of T cell stimulation in chronic infections is time-dependent, as cells primed at early stages of infection receive strong TCR signals and undergo terminal differentiation, while weaker TCR stimulation at later stages induces less differentiated memory-like T cells. Because we observed enhanced activation of CD8^{+} T cells upon IL-10R blockade, we conclude that IL-10 limits excessive T cell stimulation, most likely because of its ability to decrease TCR sensitivity to antigens (Smith et al., 2018), and thereby induces a T cell state that resembles memory cells. While transient blockade of IL-10R-STAT3 signaling increased T cell function, prolonged loss of this signaling pathway altered chromatin accessibility of T cells and promoted activity of NFAT, a key downstream mediator of TCR signaling. When acting together with AP-1, NFAT induces full T cell activation, yet when functioning alone, it promotes T cell anergy and exhaustion (Martinez et al., 2015). Our ATAC-seq data indicated that IL-10R signaling maintains NFAT:AP-1 cooperativity and thereby prevents terminal exhaustion of CD8^{+} T cells. The maintenance of the precursor memory-like PD-1^{int} TCF-1^{+} population by IL-10 represents another feature that these cells share with memory T cells. IL-10 signaling promotes memory CD8^{+} T cell maturation in acute infections as it shields them from the surrounding inflammatory milieu and thus rescues them from activation-induced terminal differentiation (Cui et al., 2011; Foulds et al., 2006; Laidlaw et al., 2015). A similar immunoregulatory role exists for PD-1, as its genetic deletion results in uncontrolled activation and loss of the TCF-1^{+} progenitor subset, leading to deteriorated function and subsequent apoptosis of virus-specific CD8^{+} T cells (Chen et al., 2019; Odorizzi et al., 2015). Conversely, persistent activation of CD8^{+} T cells by TCR or inflammatory signals, such as IFNα and IL-2, promotes T cell exhaustion and the loss of TCF-1^{+} progenitor cells (Liu et al., 2021; Wu et al., 2016). Taken together, these observations support the view that the differentiation program acquired by T cells in chronic conditions, including upregulation of immunosuppressive molecules, is evolutionarily designed to maintain adequate antigen control without causing excessive tissue damage or compromising the endurance of antigen-specific T cells (Speiser et al., 2014). Accordingly, immunoregulatory players, such as IL-10 and PD-1, have a seemingly opposite role in the long-term preservation of immune responses to chronic antigens.

CD8^{+} T cells mount anti-tumor activity in murine models of CLL (Hanna et al., 2019), and immune checkpoint blockade and other immunotherapeutic approaches lead to a substantial improvement in disease control in mice (Hanna et al., 2021; McClanahan et al., 2015; Sadik et al., 2020). Objective responses to αPD-1 or chimeric antigen receptor (CAR) T cell therapy are, however, observed only in a fraction of CLL patients (Ding et al., 2017; Porter et al., 2015) whereas the majority show resistance to these treatments (Ding et al., 2017; Fraietta et al., 2018). While this resistance is multifactorial and still requires thorough investigation, our current data suggest that modulating the IL-10R-STAT3 pathway can enhance the efficacy of immunotherapy in CLL. Stable forms of IL-10 elicit anti-tumoral immune responses in mouse models and cancer patients (Guo et al., 2021; Mumm et al., 2011; Naing et al., 2016; Qiao et al., 2019), and these responses in patients correlate with systemic and intratumoral CD8^{+} T cell activation (Naing et al., 2018). This goes in line with our observation that high *IL10* gene expression correlated with improved outcome in patients with CLL, which confirms results of a previous study (Sjöberg et al., 1996). But the fact that CLL cells themselves are a major source of IL-10 raises the question of whether systemic application of IL-10 is an appropriate treatment approach in this malignancy.

Please cite this article in press as: Hanna et al., Interleukin-10 receptor signaling promotes the maintenance of a PD-1^{int} TCF-1^{+} CD8^{+} T cell population that sustains anti-tumor immunity, Immunity (2021), https://doi.org/10.1016/j.immuni.2021.11.004

Alternatively, targeted approaches with cytokine-antibody conjugates that deliver IL-10 specifically to CD8^{+} T cells or genetically modified T cells (e.g., CAR T cells) with enhanced IL-10R-STAT3 activity seem to be a more promising strategy. Along this line, a beneficial role of STAT3 signaling in increasing the durability and success rate of CAR T cell therapy in CLL is suggested (Fraietta et al., 2018).

Altogether, the current study suggests that combination strategies involving IL-10 can enhance the efficacy of immunotherapy in CLL and beyond in other cancer types.

Limitations of the study

A major conceptual question that remains open is why IL-10 acts, on the one side, as an immunosuppressive cytokine and, on the other side, maintains anti-tumor immunity. We speculate that this is due to the divergent role of IL-10 in modulating T cell activity at different stages of an immune response, being first a driver and later a break to avoid excessive immune-mediated tissue damage. Considering this and also the tightly regulated expression and broad source of IL-10 during immune responses, it will be challenging to exploit the IL-10R-STAT3 pathway therapeutically. Unraveling the molecular link between STAT3 and the activity of NFAT:AP-1 will be of importance to overcome this challenge. In addition, an in-depth characterization of the immune microenvironment in cancer, e.g., by scRNA-seq, will help to better understand and predict which patients likely benefit from IL-10-based therapeutic approaches.

STAR★METHODS

Detailed methods are provided in the online version of this paper and include the following:

- KEY RESOURCES TABLE
- RESOURCE AVAILABILITY
  - Lead contact
  - Materials availability
  - Data and code availability
- EXPERIMENTAL MODEL AND SUBJECT DETAILS
  - Human samples
  - Mice and tumor models
- METHOD DETAILS
  - Antibody treatment
  - Collection of tissue samples and preparation of cell suspensions
  - Flow cytometry
  - Analysis of functional capacity of CD8^{+} T cells ex vivo
  - CD8^{+} T cell:CLL cell conjugation and immunological synapse assays
  - Analysis of TCR activity and T cell proliferation of CD8^{+} T cells ex vivo
  - Microarray data analysis of CD8^{+} T cells
  - Single-cell RNA-seq of CD3^{+} T cells and PD-1^{+} CD8^{+} T cells from splenocytes of TCL1 AT mouse model
  - Single-cell RNA-seq data processing and analysis
  - Computational separation of CD3^{+} T cells into CD8^{+} and CD4^{+} cells
  - V(D)J T cell analysis
  - Single-cell trajectory analysis
  - Single-cell RNA-seq analysis of breast cancer samples
  - Bulk TCR-sequencing
  - ATAC-seq library construction
  - ATAC-seq data analysis
  - ATAC-seq footprinting
  - Correlation of IL-10 expression with patient outcome
- QUANTIFICATION AND STATISTICAL ANALYSIS
  - Statistical analysis

SUPPLEMENTAL INFORMATION

Supplemental information can be found online at https://doi.org/10.1016/j.immuni.2021.11.004.

ACKNOWLEDGMENTS

We thank Dietmar Zehn (Technical University of Munich, Germany) for scientific discussions and input and Christoph Schiffler (DKFZ) for experimental support. Thanks also to the Central Animal Laboratory, the Single-cell Open Lab, and the Genomics and Proteomics Core Facility at the DKFZ, to the Nikon Imaging Facility at King's College London for technical assistance, and to Michael Hain for computational support. We further thank Ulrike Träger (DKFZ) for editing the material and methods part of this manuscript and Clemens Neufert (University Clinic Erlangen, Germany) and Ekaterina Lupar (Max Planck Institute of Immunobiology and Epigenetics, Freiburg, Germany) for providing *Stat3*-deficient and FIR × *tiger* mice, respectively.

This study was supported by the German Research Foundation (DFG) project EV-RNA (SE 2331/2-1), by the Eurostars project E!10865 - LeukeMab (01QE1716), funded by the German Ministry of Education and Research (BMBF), by the German José Carreras Foundation (grant 13R/2018) to M. Seiffert, by the German Cancer Aid to M. Seiffert (grant no. 70114114) and to P.M.R. (grant no. 112069), by an NCT 3.0 funding program (NCT3.0_2015.13 ImmunOmics, NCT3.0_2015.2 SPL/RP) to M. Schmidt and R.G., by a grant from Ministerio de Ciencia e Innovación and ERDF (SAF15-67633-R) to D.C., by the "la Caixa" Foundation (CLLEvolution-LCF/PR/HR17/52150017, Health Research 2017 Program HR17-00221) and the European Research Council (ERC) under the European Union's Horizon 2020 research and innovation program (grant agreement No 810287, BCLLatlas) to E.C., by the DFG (SFB1074 project B1) to St.St., by a grant from the ERC (ERC-CoG, #648145 REGiREG) to M.F., and by the BMBF-Network "PRECiSe" (031L0076A) and the ERA-NET TRANSCAN-2 program JTC 2014–project FIRE-CLL to St.St., P.L., and M. Seiffert.

The graphical abstract was created using BioRender.com.

AUTHOR CONTRIBUTIONS

B.S.H. designed the study, performed experiments, analyzed data, generated figures, and wrote the paper. L.L-C. was involved in the conceptual design of the study, performed experiments, analyzed data, generated figures, and wrote the paper. M.I. performed bioinformatical analyses, generated figures, and wrote parts of the paper. P.M.R. performed experiments, analyzed data, and generated figures. J.K.L.W. and Y.P. analyzed scRNA-seq data and generated figures. L.C.K. and K.R. performed ATAC-seq, analyzed data, and generated figures. K.R. helped with editing the text. N.I. and A.G.R. performed cell conjugation and immunological synapse assays, analyzed data, and generated figures. S.Ö., N.M., and V.K. conducted experiments. D.C., E.C., J.B., St.St., and S.D. provided clinical samples and information and performed correlation analyses. M. Schmidt and R.G. performed TCR sequencing, analyzed data, and generated figures. M.F. was involved in discussions regarding experimental protocols and data, as well as in paper writing. P.L. provided logistic and budget support and was involved in discussions and paper writing. M.Z. performed and supervised bioinformatical analyses and interpreted and discussed data. M. Seiffert designed the study, interpreted and discussed data, provided logistic and budget support, and wrote the paper.

DECLARATION OF INTERESTS

The authors declare no competing interests.

INCLUSION AND DIVERSITY

One or more of the authors of this paper self-identifies as an underrepresented ethnic minority in science.

Received: January 9, 2021
Revised: March 26, 2021
Accepted: November 9, 2021
Published: December 7, 2021

REFERENCES

Adey, A., Morrison, H.G., Asan, Xun, X., Kitzman, J.O., Turner, E.H., Stackhouse, B., MacKenzie, A.P., Caruccio, N.C., Zhang, X., and Shendure, J. (2010). Rapid, low-input, low-bias construction of shotgun fragment libraries by high-density in vitro transposition. Genome Biol. *11*, R119.

Afzal, S., Gil-Farina, I., Gabriel, R., Ahmad, S., von Kalle, C., Schmidt, M., and Fronza, R. (2019). Systematic comparative study of computational methods for T-cell receptor sequencing data analysis. Brief. Bioinform. *20*, 222–234.

Alquicira-Hernandez, J., and Powell, J.E. (2021). Nebulosa recovers single cell gene expression signals by kernel density estimation. Bioinformatics, btab003.

Azizi, E., Carr, A.J., Plitas, G., Cornish, A.E., Konopacki, C., Prabhakaran, S., Nainys, J., Wu, K., Kiseliovas, V., Setty, M., et al. (2018). Single-Cell Map of Diverse Immune Phenotypes in the Breast Tumor Microenvironment. Cell *174*, 1293–1308.e36.

Beltra, J.-C., Manne, S., Abdel-Hakeem, M.S., Kurachi, M., Giles, J.R., Chen, Z., Casella, V., Ngiow, S.F., Khan, O., Huang, Y.J., et al. (2020). Developmental Relationships of Four Exhausted CD8^{+} T Cell Subsets Reveals Underlying Transcriptional and Epigenetic Landscape Control Mechanisms. Immunity *52*, 825–841.e8.

Bengtsson, H., Simpson, K., Bullard, J., and Hansen, K. (2008). aroma.affymetrix: A generic framework in R for analyzing small to very large Affymetrix data sets in bounded memory.

Betts, M.R., Brenchley, J.M., Price, D.A., De Rosa, S.C., Douek, D.C., Roederer, M., and Koup, R.A. (2003). Sensitive and viable identification of antigen-specific CD8+ T cells by a flow cytometric assay for degranulation. J. Immunol. Methods *281*, 65–78.

Bichi, R., Shinton, S.A., Martin, E.S., Koval, A., Calin, G.A., Cesari, R., Russo, G., Hardy, R.R., and Croce, C.M. (2002). Human chronic lymphocytic leukemia modeled in mouse by targeted TCL1 expression. Proc. Natl. Acad. Sci. USA *99*, 6955–6960.

Blackburn, S.D., Shin, H., Freeman, G.J., and Wherry, E.J. (2008). Selective expansion of a subset of exhausted CD8 T cells by alphaPD-L1 blockade. Proc. Natl. Acad. Sci. USA *105*, 15016–15021.

Blazar, B.R., Taylor, P.A., Panoskaltsis-Mortari, A., Narula, S.K., Smith, S.R., Roncarolo, M.G., and Vallera, D.A. (1998). Interleukin-10 dose-dependent regulation of CD4+ and CD8+ T cell-mediated graft-versus-host disease. Transplantation *66*, 1220–1229.

Bolger, A.M., Lohse, M., and Usadel, B. (2014). Trimmomatic: a flexible trimmer for Illumina sequence data. Bioinformatics *30*, 2114–2120.

Bolotin, D.A., Poslavsky, S., Mitrophanov, I., Shugay, M., Mamedov, I.Z., Putintseva, E.V., and Chudakov, D.M. (2015). MiXCR: software for comprehensive adaptive immunity profiling. Nat. Methods *12*, 380–381.

Brooks, D.G., Trifilo, M.J., Edelmann, K.H., Teyton, L., McGavern, D.B., and Oldstone, M.B. (2006). Interleukin-10 determines viral clearance or persistence in vivo. Nat. Med. *12*, 1301–1309.

Buenrostro, J.D., Giresi, P.G., Zaba, L.C., Chang, H.Y., and Greenleaf, W.J. (2013). Transposition of native chromatin for fast and sensitive epigenomic profiling of open chromatin, DNA-binding proteins and nucleosome position. Nat. Methods *10*, 1213–1218.

Butler, A., Hoffman, P., Smibert, P., Papalexi, E., and Satija, R. (2018). Integrating single-cell transcriptomic data across different conditions, technologies, and species. Nat. Biotechnol. *36*, 411–420.

Cao, J., Spielmann, M., Qiu, X., Huang, X., Ibrahim, D.M., Hill, A.J., Zhang, F., Mundlos, S., Christiansen, L., Steemers, F.J., et al. (2019). The single-cell transcriptional landscape of mammalian organogenesis. Nature *566*, 496–502.

Carlson, M., and Maintainer, B. (2015). TxDb.Mmusculus.UCSC.mm9.knownGene: Annotation package for TxDb object(s). (R package), version 3.2.2.

Chen, Z., Ji, Z., Ngiow, S.F., Manne, S., Cai, Z., Huang, A.C., Johnson, J., Staupe, R.P., Bengsch, B., Xu, C., et al. (2019). TCF-1-Centered Transcriptional Network Drives an Effector versus Exhausted CD8 T Cell-Fate Decision. Immunity *51*, 840–855.e5.

Cui, W., Liu, Y., Weinstein, J.S., Craft, J., and Kaech, S.M. (2011). An interleukin-21-interleukin-10-STAT3 pathway is critical for functional maturation of memory CD8+ T cells. Immunity *35*, 792–805.

Dietrich, S., Oleś, M., Lu, J., Sellner, L., Anders, S., Velten, B., Wu, B., Hüllein, J., da Silva Liberio, M., Walther, T., et al. (2018). Drug-perturbation-based stratification of blood cancer. J. Clin. Invest. *128*, 427–445.

DiLillo, D.J., Weinberg, J.B., Yoshizaki, A., Horikawa, M., Bryant, J.M., Iwata, Y., Matsushita, T., Matta, K.M., Chen, Y., Venturi, G.M., et al. (2013). Chronic lymphocytic leukemia and regulatory B cells share IL-10 competence and immunosuppressive function. Leukemia *27*, 170–182.

Ding, W., LaPlant, B.R., Call, T.G., Parikh, S.A., Leis, J.F., He, R., Shanafelt, T.D., Sinha, S., Le-Rademacher, J., Feldman, A.L., et al. (2017). Pembrolizumab in patients with CLL and Richter transformation or with relapsed CLL. Blood *129*, 3419–3427.

Dobin, A., Davis, C.A., Schlesinger, F., Drenkow, J., Zaleski, C., Jha, S., Batut, P., Chaisson, M., and Gingeras, T.R. (2013). STAR: ultrafast universal RNA-seq aligner. Bioinformatics *29*, 15–21.

Doering, T.A., Crawford, A., Angelosanto, J.M., Paley, M.A., Ziegler, C.G., and Wherry, E.J. (2012). Network analysis reveals centrally connected genes and pathways involved in CD8+ T cell exhaustion versus memory. Immunity *37*, 1130–1144.

Durinck, S., Spellman, P.T., Birney, E., and Huber, W. (2009). Mapping identifiers for the integration of genomic datasets with the R/Bioconductor package biomaRt. Nat. Protoc. *4*, 1184–1191.

Ejrnaes, M., Filippi, C.M., Martinic, M.M., Ling, E.M., Togher, L.M., Crotty, S., and von Herrath, M.G. (2006). Resolution of a chronic viral infection after interleukin-10 receptor blockade. J. Exp. Med. *203*, 2461–2472.

Emmerich, J., Mumm, J.B., Chan, I.H., LaFace, D., Truong, H., McClanahan, T., Gorman, D.M., and Oft, M. (2012). IL-10 directly activates and expands tumor-resident CD8(+) T cells without de novo infiltration from secondary lymphoid organs. Cancer Res. *72*, 3570–3581.

Fayad, L., Keating, M.J., Reuben, J.M., O'Brien, S., Lee, B.N., Lerner, S., and Kurzrock, R. (2001). Interleukin-6 and interleukin-10 levels in chronic lymphocytic leukemia: correlation with phenotypic characteristics and outcome. Blood *97*, 256–263.

Finbloom, D.S., and Winestock, K.D. (1995). IL-10 induces the tyrosine phosphorylation of tyk2 and Jak1 and the differential assembly of STAT1 alpha and STAT3 complexes in human T cells and monocytes. J. Immunol. *155*, 1079–1090.

Foulds, K.E., Rotte, M.J., and Seder, R.A. (2006). IL-10 is required for optimal CD8 T cell memory following Listeria monocytogenes infection. J. Immunol. *177*, 2565–2574.

Fraietta, J.A., Lacey, S.F., Orlando, E.J., Pruteanu-Malinici, I., Gohil, M., Lundh, S., Boesteanu, A.C., Wang, Y., O'Connor, R.S., Hwang, W.-T., et al. (2018). Determinants of response and resistance to CD19 chimeric antigen receptor (CAR) T cell therapy of chronic lymphocytic leukemia. Nat. Med. *24*, 563–571.

Gentleman, R.C., Carey, V.J., Bates, D.M., Bolstad, B., Dettling, M., Dudoit, S., Ellis, B., Gautier, L., Ge, Y., Gentry, J., et al. (2004). Bioconductor: open software development for computational biology and bioinformatics. Genome Biol. *5*, R80.

Groux, H., Bigler, M., de Vries, J.E., and Roncarolo, M.G. (1998). Inhibitory and stimulatory effects of IL-10 on human CD8þ T cells. J. Immunol. *160*, 3188–3193.

Guo, Y., Xie, Y.Q., Gao, M., Zhao, Y., Franco, F., Wenes, M., Siddiqui, I., Bevilacqua, A., Wang, H., Yang, H., et al. (2021). Metabolic reprogramming of terminally exhausted CD8^{+} T cells by IL-10 enhances anti-tumor immunity. Nat. Immunol. *22*, 746–756.

Hamid, O., Robert, C., Daud, A., Hodi, F.S., Hwu, W.J., Kefford, R., Wolchok, J.D., Hersey, P., Joseph, R.W., Weber, J.S., et al. (2013). Safety and tumor responses with lambrolizumab (anti-PD-1) in melanoma. N. Engl. J. Med. *369*, 134–144.

Hanna, B.S., McClanahan, F., Yazdanparast, H., Zaborsky, N., Kalter, V., Rößner, P.M., Benner, A., Dürr, C., Egle, A., Gribben, J.G., et al. (2016). Depletion of CLL-associated patrolling monocytes and macrophages controls disease development and repairs immune dysfunction in vivo. Leukemia *30*, 570–579.

Hanna, B.S., Roessner, P.M., Yazdanparast, H., Colomer, D., Campo, E., Kugler, S., Yosifov, D., Stilgenbauer, S., Schmidt, M., Gabriel, R., et al. (2019). Control of chronic lymphocytic leukemia development by clonally-expanded CD8^{+} T-cells that undergo functional exhaustion in secondary lymphoid tissues. Leukemia *33*, 625–637.

Hanna, B.S., Yazdanparast, H., Demerdash, Y., Roessner, P.M., Schulz, R., Lichter, P., Stilgenbauer, S., and Seiffert, M. (2021). Combining ibrutinib and checkpoint blockade improves CD8+ T-cell function and control of chronic lymphocytic leukemia in Em-TCL1 mice. Haematologica *106*, 968–977.

Hao, Y., Hao, S., Andersen-Nissen, E., Mauck, W.M., III, Zheng, S., Butler, A., Lee, M.J., Wilk, A.J., Darby, C., Zager, M., et al. (2021). Integrated analysis of multimodal single-cell data. Cell *13*, 3573–3587.

Heinz, S., Benner, C., Spann, N., Bertolino, E., Lin, Y.C., Laslo, P., Cheng, J.X., Murre, C., Singh, H., and Glass, C.K. (2010). Simple combinations of lineage-determining transcription factors prime cis-regulatory elements required for macrophage and B cell identities. Mol. Cell *38*, 576–589.

Hofbauer, J.P., Heyder, C., Denk, U., Kocher, T., Holler, C., Trapin, D., Asslaber, D., Tinhofer, I., Greil, R., and Egle, A. (2011). Development of CLL in the TCL1 transgenic mouse model is associated with severe skewing of the T-cell compartment homologous to human CLL. Leukemia *25*, 1452–1458.

Hudson, W.H., Gensheimer, J., Hashimoto, M., Wieland, A., Valanparambil, R.M., Li, P., Lin, J.X., Konieczny, B.T., Im, S.J., Freeman, G.J., et al. (2019). Proliferating Transitory T Cells with an Effector-like Transcriptional Signature Emerge from PD-1^{+} Stem-like CD8^{+} T Cells during Chronic Infection. Immunity *51*, 1043–1058.e4.

Im, S.J., Hashimoto, M., Gerner, M.Y., Lee, J., Kissick, H.T., Burger, M.C., Shan, Q., Hale, J.S., Lee, J., Nasti, T.H., et al. (2016). Defining CD8+ T cells that provide the proliferative burst after PD-1 therapy. Nature *537*, 417–421.

Irizarry, R.A., Bolstad, B.M., Collin, F., Cope, L.M., Hobbs, B., and Speed, T.P. (2003). Summaries of Affymetrix GeneChip probe level data. Nucleic Acids Res. *31*, e15.

Jiang, Y., Li, Y., and Zhu, B. (2015). T-cell exhaustion in the tumor microenvironment. Cell Death Dis. *6*, e1792.

Kamanaka, M., Kim, S.T., Wan, Y.Y., Sutterwala, F.S., Lara-Tejero, M., Galán, J.E., Harhaj, E., and Flavell, R.A. (2006). Expression of interleukin-10 in intestinal lymphocytes detected by an interleukin-10 reporter knockin tiger mouse. Immunity *25*, 941–952.

Kanehisa, M., and Goto, S. (2000). KEGG: kyoto encyclopedia of genes and genomes. Nucleic Acids Res. *28*, 27–30.

Laidlaw, B.J., Cui, W., Amezquita, R.A., Gray, S.M., Guan, T., Lu, Y., Kobayashi, Y., Flavell, R.A., Kleinstein, S.H., Craft, J., and Kaech, S.M. (2015). Production of IL-10 by CD4(+) regulatory T cells during the resolution of infection promotes the maturation of memory CD8(+) T cells. Nat. Immunol. *16*, 871–879.

Langmead, B., and Salzberg, S.L. (2012). Fast gapped-read alignment with Bowtie 2. Nat. Methods *9*, 357–359.

Li, H., Handsaker, B., Wysoker, A., Fennell, T., Ruan, J., Homer, N., Marth, G., Abecasis, G., and Durbin, R.; 1000 Genome Project Data Processing Subgroup (2009). The Sequence Alignment/Map format and SAMtools. Bioinformatics *25*, 2078–2079.

Li, H., van der Leun, A.M., Yofe, I., Lubling, Y., Gelbard-Solodkin, D., van Akkooi, A.C.J., van den Braber, M., Rozeman, E.A., Haanen, J.B.A.G., Blank, C.U., et al. (2019). Dysfunctional CD8 T Cells Form a Proliferative, Dynamically Regulated Compartment within Human Melanoma. Cell *176*, 775–789.e18.

Liberzon, A., Subramanian, A., Pinchback, R., Thorvaldsdóttir, H., Tamayo, P., and Mesirov, J.P. (2011). Molecular signatures database (MSigDB) 3.0. Bioinformatics *27*, 1739–1740.

Liu, Y., Zhou, N., Zhou, L., Wang, J., Zhou, Y., Zhang, T., Fang, Y., Deng, J., Gao, Y., Liang, X., et al. (2021). IL-2 regulates tumor-reactive CD8^{+} T cell exhaustion by activating the aryl hydrocarbon receptor. Nat. Immunol. *22*, 358–369.

Lockstone, H.E. (2011). Exon array data analysis using Affymetrix power tools and R statistical software. Brief. Bioinform. *12*, 634–644.

Love, M.I., Huber, W., and Anders, S. (2014). Moderated estimation of fold change and dispersion for RNA-seq data with DESeq2. Genome Biol. *15*, 550.

Luo, W., and Brouwer, C. (2013). Pathview: an R/Bioconductor package for pathway-based data integration and visualization. Bioinformatics *29*, 1830–1831.

Man, K., Gabriel, S.S., Liao, Y., Gloury, R., Preston, S., Henstridge, D.C., Pellegrini, M., Zehn, D., Berberich-Siebelt, F., Febbraio, M.A., et al. (2017). Transcription Factor IRF4 Promotes CD8^{+} T Cell Exhaustion and Limits the Development of Memory-like T Cells during Chronic Infection. Immunity *47*, 1129–1141.e5.

Martinez, G.J., Pereira, R.M., Äijö, T., Kim, E.Y., Marangoni, F., Pipkin, M.E., Togher, S., Heissmeyer, V., Zhang, Y.C., Crotty, S., et al. (2015). The transcription factor NFAT promotes exhaustion of activated CD8^{+} T cells. Immunity *42*, 265–278.

McClanahan, F., Hanna, B., Miller, S., Clear, A.J., Lichter, P., Gribben, J.G., and Seiffert, M. (2015). PD-L1 checkpoint blockade prevents immune dysfunction and leukemia development in a mouse model of chronic lymphocytic leukemia. Blood *126*, 203–211.

McLane, L.M., Abdel-Hakeem, M.S., and Wherry, E.J. (2019). CD8 T Cell Exhaustion During Chronic Viral Infection and Cancer. Annu. Rev. Immunol. *37*, 457–495.

McLean, C.Y., Bristor, D., Hiller, M., Clarke, S.L., Schaar, B.T., Lowe, C.B., Wenger, A.M., and Bejerano, G. (2010). GREAT improves functional interpretation of cis-regulatory regions. Nat. Biotechnol. *28*, 495–501.

Miller, B.C., Sen, D.R., Al Abosy, R., Bi, K., Virkud, Y.V., LaFleur, M.W., Yates, K.B., Lako, A., Felt, K., Naik, G.S., et al. (2019). Subsets of exhausted CD8^{+} T cells differentially mediate tumor control and respond to checkpoint blockade. Nat. Immunol. *20*, 326–336.

Montraveta, A., Lee-Vergés, E., Roldán, J., Jiménez, L., Cabezas, S., Clot, G., Pinyol, M., Xargay-Torrent, S., Rosich, L., Arimany-Nardí, C., et al. (2016). CD69 expression potentially predicts response to bendamustine and its modulation by ibrutinib or idelalisib enhances cytotoxic effect in chronic lymphocytic leukemia. Oncotarget *7*, 5507–5520.

Moore, K.W., de Waal Malefyt, R., Coffman, R.L., and O'Garra, A. (2001). Interleukin-10 and the interleukin-10 receptor. Annu. Rev. Immunol. *19*, 683–765.

Mumm, J.B., Emmerich, J., Zhang, X., Chan, I., Wu, L., Mauze, S., Blaisdell, S., Basham, B., Dai, J., Grein, J., et al. (2011). IL-10 elicits IFNγ-dependent tumor immune surveillance. Cancer Cell *20*, 781–796.

Naing, A., Papadopoulos, K.P., Autio, K.A., Ott, P.A., Patel, M.R., Wong, D.J., Falchook, G.S., Pant, S., Whiteside, M., Rasco, D.R., et al. (2016). Safety, Antitumor Activity, and Immune Activation of Pegylated Recombinant Human Interleukin-10 (AM0010) in Patients With Advanced Solid Tumors. J. Clin. Oncol. *34*, 3562–3569.

Naing, A., Infante, J.R., Papadopoulos, K.P., Chan, I.H., Shen, C., Ratti, N.P., Rojo, B., Autio, K.A., Wong, D.J., Patel, M.R., et al. (2018). PEGylated IL-10 (Pegilodecakin) Induces Systemic Immune Activation, CD8^{+} T Cell

Invigoration and Polyclonal T Cell Expansion in Cancer Patients. Cancer Cell *34*, 775–791.e3.

Neven, B., Mamessier, E., Bruneau, J., Kaltenbach, S., Kotlarz, D., Suarez, F., Masliah-Planchon, J., Billot, K., Canioni, D., Frange, P., et al. (2013). A Mendelian predisposition to B-cell lymphoma caused by IL-10R deficiency. Blood *122*, 3713–3722.

Nizzoli, G., Larghi, P., Paroni, M., Crosti, M.C., Moro, M., Neddermann, P., Caprioli, F., Pagani, M., De Francesco, R., Abrignani, S., and Geginat, J. (2016). IL-10 promotes homeostatic proliferation of human CD8(+) memory T cells and, when produced by CD1c(+) DCs, shapes naive CD8(+) T-cell priming. Eur. J. Immunol. *46*, 1622–1632.

O'Garra, A., and Vieira, P. (2007). T(H)1 cells control themselves by producing interleukin-10. Nat. Rev. Immunol. *7*, 425–428.

Odorizzi, P.M., Pauken, K.E., Paley, M.A., Sharpe, A., and Wherry, E.J. (2015). Genetic absence of PD-1 promotes accumulation of terminally differentiated exhausted CD8+ T cells. J. Exp. Med. *212*, 1125–1137.

Paley, M.A., Kroy, D.C., Odorizzi, P.M., Johnnidis, J.B., Dolfi, D.V., Barnett, B.E., Bikoff, E.K., Robertson, E.J., Lauer, G.M., Reiner, S.L., and Wherry, E.J. (2012). Progenitor and terminal subsets of CD8+ T cells cooperate to contain chronic viral infection. Science *338*, 1220–1225.

Parish, I.A., Marshall, H.D., Staron, M.M., Lang, P.A., Brüstle, A., Chen, J.H., Cui, W., Tsui, Y.C., Perry, C., Laidlaw, B.J., et al. (2014). Chronic viral infection promotes sustained Th1-derived immunoregulatory IL-10 via BLIMP-1. J. Clin. Invest. *124*, 3455–3468.

Pauken, K.E., and Wherry, E.J. (2015). Overcoming T cell exhaustion in infection and cancer. Trends Immunol. *36*, 265–276.

Pique-Regi, R., Degner, J.F., Pai, A.A., Gaffney, D.J., Gilad, Y., and Pritchard, J.K. (2011). Accurate inference of transcription factor binding from DNA sequence and chromatin accessibility data. Genome Res. *21*, 447–455.

Porter, D.L., Hwang, W.-T., Frey, N.V., Lacey, S.F., Shaw, P.A., Loren, A.W., Bagg, A., Marcucci, K.T., Shen, A., Gonzalez, V., et al. (2015). Chimeric antigen receptor T cells persist and induce sustained remissions in relapsed refractory chronic lymphocytic leukemia. Sci. Transl. Med. *7*, 303ra139.

Qiao, J., Liu, Z., Dong, C., Luan, Y., Zhang, A., Moore, C., Fu, K., Peng, J., Wang, Y., Ren, Z., et al. (2019). Targeting Tumors with IL-10 Prevents Dendritic Cell-Mediated CD8^{+} T Cell Apoptosis. Cancer Cell *35*, 901–915.e4.

Qiu, X., Mao, Q., Tang, Y., Wang, L., Chawla, R., Pliner, H.A., and Trapnell, C. (2017). Reversed graph embedding resolves complex single-cell trajectories. Nat. Methods *14*, 979–982.

Quigley, M., Pereyra, F., Nilsson, B., Porichis, F., Fonseca, C., Eichbaum, Q., Julg, B., Jesneck, J.L., Brosnahan, K., Imam, S., et al. (2010). Transcriptional analysis of HIV-specific CD8+ T cells shows that PD-1 inhibits T cell function by upregulating BATF. Nat. Med. *16*, 1147–1151.

Ramsay, A.G., Johnson, A.J., Lee, A.M., Gorgün, G., Le Dieu, R., Blum, W., Byrd, J.C., and Gribben, J.G. (2008). Chronic lymphocytic leukemia T cells show impaired immunological synapse formation that can be reversed with an immunomodulating drug. J. Clin. Invest. *118*, 2427–2437.

Ray, J.P., Marshall, H.D., Laidlaw, B.J., Staron, M.M., Kaech, S.M., and Craft, J. (2014). Transcription factor STAT3 and type I interferons are corepressive insulators for differentiation of follicular helper and T helper 1 cells. Immunity *40*, 367–377.

Ross-Innes, C.S., Stark, R., Teschendorff, A.E., Holmes, K.A., Ali, H.R., Dunning, M.J., Brown, G.D., Gojis, O., Ellis, I.O., Green, A.R., et al. (2012). Differential oestrogen receptor binding is associated with clinical outcome in breast cancer. Nature *481*, 389–393.

Ruffell, B., Chang-Strachan, D., Chan, V., Rosenbusch, A., Ho, C.M., Pryer, N., Daniel, D., Hwang, E.S., Rugo, H.S., and Coussens, L.M. (2014). Macrophage IL-10 blocks CD8+ T cell-dependent responses to chemotherapy by suppressing IL-12 expression in intratumoral dendritic cells. Cancer Cell *26*, 623–637.

Ruggiero, E., Nicolay, J.P., Fronza, R., Arens, A., Paruzynski, A., Nowrouzi, A., Ürenden, G., Lulay, C., Schneider, S., Goerdt, S., et al. (2015). High-resolution analysis of the human T-cell receptor repertoire. Nat. Commun. *6*, 8081.

Sadik, A., Somarribas Patterson, L.F., Öztürk, S., Mohapatra, S.R., Panitz, V., Secker, P.F., Pfänder, P., Loth, S., Salem, H., Prentzell, M.T., et al. (2020). IL4I1 Is a Metabolic Immune Checkpoint that Activates the AHR and Promotes Tumor Progression. Cell *182*, 1252–1270.e34.

Sarkar, S., Kalia, V., Haining, W.N., Konieczny, B.T., Subramaniam, S., and Ahmed, R. (2008). Functional and genomic profiling of effector CD8 T cell subsets with distinct memory fates. J. Exp. Med. *205*, 625–640.

Sawant, D.V., Yano, H., Chikina, M., Zhang, Q., Liao, M., Liu, C., Callahan, D.J., Sun, Z., Sun, T., Tabib, T., et al. (2019). Adaptive plasticity of IL-10^{+} and IL-35^{+} T_{reg} cells cooperatively promotes tumor T cell exhaustion. Nat. Immunol. *20*, 724–735.

Schietinger, A., Philip, M., Krisnawan, V.E., Chiu, E.Y., Delrow, J.J., Basom, R.S., Lauer, P., Brockstedt, D.G., Knoblaugh, S.E., Hämmerling, G.J., et al. (2016). Tumor-Specific T Cell Dysfunction Is a Dynamic Antigen-Driven Differentiation Program Initiated Early during Tumorigenesis. Immunity *45*, 389–401.

Scott-Browne, J.P., López-Moyado, I.F., Trifari, S., Wong, V., Chavez, L., Rao, A., and Pereira, R.M. (2016). Dynamic Changes in Chromatin Accessibility Occur in CD8^{+} T Cells Responding to Viral Infection. Immunity *45*, 1327–1340.

Sen, D.R., Kaminski, J., Barnitz, R.A., Kurachi, M., Gerdemann, U., Yates, K.B., Tsao, H.-W., Godec, J., LaFleur, M.W., Brown, F.D., et al. (2016). The epigenetic landscape of T cell exhaustion. Science *354*, 1165–1169.

Shannon, C.E. (1997). The mathematical theory of communication. 1963. MD Comput. *14*, 306–317.

Shen, L., Shao, N., Liu, X., and Nestler, E. (2014). ngs.plot: Quick mining and visualization of next-generation sequencing data by integrating genomic databases. BMC Genomics *15*, 284.

Shin, H., Blackburn, S.D., Intlekofer, A.M., Kao, C., Angelosanto, J.M., Reiner, S.L., and Wherry, E.J. (2009). A role for the transcriptional repressor Blimp-1 in CD8(+) T cell exhaustion during chronic viral infection. Immunity *31*, 309–320.

Shinkai, Y., Rathbun, G., Lam, K.P., Oltz, E.M., Stewart, V., Mendelsohn, M., Charron, J., Datta, M., Young, F., Stall, A.M., et al. (1992). RAG-2-deficient mice lack mature lymphocytes owing to inability to initiate V(D)J rearrangement. Cell *68*, 855–867.

Shugay, M., Bagaev, D.V., Turchaninova, M.A., Bolotin, D.A., Britanova, O.V., Putintseva, E.V., Pogorelyy, M.V., Nazarov, V.I., Zvyagin, I.V., Kirgizova, V.I., et al. (2015). VDJtools: Unifying Post-analysis of T Cell Receptor Repertoires. PLoS Comput. Biol. *11*, e1004503.

Sjöberg, J., Aguilar-Santelises, M., Sjögren, A.M., Pisa, E.K., Ljungdahl, A., Björkholm, M., Jondal, M., Mellstedt, H., and Pisa, P. (1996). Interleukin-10 mRNA expression in B-cell chronic lymphocytic leukaemia inversely correlates with progression of disease. Br. J. Haematol. *92*, 393–400.

Smith, L.K., Boukhaled, G.M., Condotta, S.A., Mazouz, S., Guthmiller, J.J., Vijay, R., Butler, N.S., Bruneau, J., Shoukry, N.H., Krawczyk, C.M., and Richer, M.J. (2018). Interleukin-10 Directly Inhibits CD8^{+} T Cell Function by Enhancing N-Glycan Branching to Decrease Antigen Sensitivity. Immunity *48*, 299–312.e5.

Smyth, G.K. (2004). Linear models and empirical bayes methods for assessing differential expression in microarray experiments. Stat. Appl. Genet. Mol. Biol. *3*, e3.

Snell, L.M., MacLeod, B.L., Law, J.C., Osokine, I., Elsaesser, H.J., Hezaveh, K., Dickson, R.J., Gavin, M.A., Guidos, C.J., McGaha, T.L., and Brooks, D.G. (2018). CD8^{+} T Cell Priming in Established Chronic Viral Infection Preferentially Directs Differentiation of Memory-like Cells for Sustained Immunity. Immunity *49*, 678–694.e5.

Speiser, D.E., Utzschneider, D.T., Oberle, S.G., Münz, C., Romero, P., and Zehn, D. (2014). T cell differentiation in chronic infection and cancer: functional adaptation or exhaustion? Nat. Rev. Immunol. *14*, 768–774.

Stilgenbauer, S., Zenz, T., Winkler, D., Bühler, A., Schlenk, R.F., Groner, S., Busch, R., Hensel, M., Dührsen, U., Finke, J., et al.; German Chronic Lymphocytic Leukemia Study Group (2009). Subcutaneous alemtuzumab in fludarabine-refractory chronic lymphocytic leukemia: clinical results and prognostic marker analyses from the CLL2H study of the German Chronic Lymphocytic Leukemia Study Group. J. Clin. Oncol. *27*, 3994–4001.

Stuart, T., Butler, A., Hoffman, P., Hafemeister, C., Papalexi, E., Mauck, W.M., 3rd, Hao, Y., Stoeckius, M., Smibert, P., and Satija, R. (2019). Comprehensive Integration of Single-Cell Data. Cell *177*, 1888–1902.e21.

Subramanian, A., Tamayo, P., Mootha, V.K., Mukherjee, S., Ebert, B.L., Gillette, M.A., Paulovich, A., Pomeroy, S.L., Golub, T.R., Lander, E.S., and Mesirov, J.P. (2005). Gene set enrichment analysis: a knowledge-based approach for interpreting genome-wide expression profiles. Proc. Natl. Acad. Sci. USA *102*, 15545–15550.

Takeda, K., Kaisho, T., Yoshida, N., Takeda, J., Kishimoto, T., and Akira, S. (1998). Stat3 activation is responsible for IL-6-dependent T cell proliferation through preventing apoptosis: generation and characterization of T cell-specific Stat3-deficient mice. J. Immunol. *161*, 4652–4660.

Thommen, D.S., Koelzer, V.H., Herzig, P., Roller, A., Trefny, M., Dimeloe, S., Kiialainen, A., Hanhart, J., Schill, C., Hess, C., et al. (2018). A transcriptionally and functionally distinct PD-1^{+} CD8^{+} T cell pool with predictive potential in non-small-cell lung cancer treated with PD-1 blockade. Nat. Med. *24*, 994–1004.

Topalian, S.L., Hodi, F.S., Brahmer, J.R., Gettinger, S.N., Smith, D.C., McDermott, D.F., Powderly, J.D., Carvajal, R.D., Sosman, J.A., Atkins, M.B., et al. (2012). Safety, activity, and immune correlates of anti-PD-1 antibody in cancer. N. Engl. J. Med. *366*, 2443–2454.

Topalian, S.L., Drake, C.G., and Pardoll, D.M. (2015). Immune checkpoint blockade: a common denominator approach to cancer therapy. Cancer Cell *27*, 450–461.

Utzschneider, D.T., Charmoy, M., Chennupati, V., Pousse, L., Ferreira, D.P., Calderon-Copete, S., Danilo, M., Alfei, F., Hofmann, M., Wieland, D., et al. (2016). T Cell Factor 1-Expressing Memory-like CD8(+) T Cells Sustain the Immune Response to Chronic Viral Infections. Immunity *45*, 415–427.

West, E.E., Youngblood, B., Tan, W.G., Jin, H.T., Araki, K., Alexe, G., Konieczny, B.T., Calpe, S., Freeman, G.J., Terhorst, C., et al. (2011). Tight regulation of memory CD8(+) T cells limits their effectiveness during sustained high viral load. Immunity *35*, 285–298.

Wherry, E.J. (2011). T cell exhaustion. Nat. Immunol. *12*, 492–499.

Wherry, E.J., Ha, S.J., Kaech, S.M., Haining, W.N., Sarkar, S., Kalia, V., Subramaniam, S., Blattman, J.N., Barber, D.L., and Ahmed, R. (2007). Molecular signature of CD8+ T cell exhaustion during chronic viral infection. Immunity *27*, 670–684.

Wickham, H., Navarro, D., and Pedersen, T.L. (2009). ggplot2: elegant graphics for data analysis (Springer).

Wu, T., Ji, Y., Moseman, E.A., Xu, H.C., Manglani, M., Kirby, M., Anderson, S.M., Handon, R., Kenyon, E., Elkahloun, A., et al. (2016). The TCF1-Bcl6 axis counteracts type I interferon to repress exhaustion and maintain T cell stemness. Sci. Immunol. *1*, eaai8593.

Yates, A., Akanni, W., Amode, M.R., Barrell, D., Billis, K., Carvalho-Silva, D., Cummins, C., Clapham, P., Fitzgerald, S., Gil, L., et al. (2016). Ensembl 2016. Nucleic Acids Res. *44* (D1), D710–D716.

Yu, G., Wang, L.-G., and He, Q.-Y. (2015). ChIPseeker: an R/Bioconductor package for ChIP peak annotation, comparison and visualization. Bioinformatics *31*, 2382–2383.

Zenz, T., Mertens, D., Küppers, R., Döhner, H., and Stilgenbauer, S. (2010). From pathogenesis to treatment of chronic lymphocytic leukaemia. Nat. Rev. Cancer *10*, 37–50.

Zhang, Y., Liu, T., Meyer, C.A., Eeckhoute, J., Johnson, D.S., Bernstein, B.E., Nusbaum, C., Myers, R.M., Brown, M., Li, W., and Liu, X.S. (2008). Model-based analysis of ChIP-Seq (MACS). Genome Biol. *9*, R137.

Zhao, S., Guo, Y., Sheng, Q., and Shyr, Y. (2014). Heatmap3: an improved heatmap package with more powerful and convenient features. BMC Bioinformatics *15*, P16.

Please cite this article in press as: Hanna et al., Interleukin-10 receptor signaling promotes the maintenance of a PD-1^{int} TCF-1^{+} CD8^{+} T cell population that sustains anti-tumor immunity, Immunity (2021), https://doi.org/10.1016/j.immuni.2021.11.004

STAR★METHODS

KEY RESOURCES TABLE

REAGENT or RESOURCE	SOURCE	IDENTIFIER
Antibodies		
Anti-human CD197 (CCR7) (clone G043H7)	Biolegend	Cat# 353235; RRID: AB_2563640, Cat# 353208; RRID: AB_11203894
Anti-human CD3 (clone OKT3)	Biolegend	Cat# 317336; RRID: AB_2561628
Anti-human CD45RO (clone UCHL1)	Biolegend	Cat# 304227; RRID: AB_10899580
Anti-human CD69 (clone FN50)	Biolegend	Cat# 310941; RRID: AB_2564276
Anti-human CD8a (clone RPA-T8)	Biolegend	Cat# 301060; RRID: AB_2564165, Cat# 301040; RRID: AB_2563185
Anti-human Granzyme B (clone GB11)	Biolegend	Cat# 515403; RRID: AB_2114575
Anti-human IFNγ (clone 4S.B3)	Biolegend	Cat# 502528; RRID: AB_2123323
Anti-human PD-1 (clone EH12.2H7)	Biolegend	Cat# 329906; RRID: AB_940483, Cat# 329918; RRID: AB_2159324, Cat# 329939; RRID: AB_2563658
Anti-mouse CD101 (clone Moushi101)	ThermoFisher	Cat# 25-1011-82; RRID: AB_2573378
Anti-mouse CD107a (LAMP-1) (clone eBio1D4B)	ThermoFisher	Cat# 12-1071-8; RRID: AB_657556
Anti-mouse CD11b (clone M1/70)	ThermoFisher	Cat# 25-0112-81; RRID: AB_469587
Anti-mouse CD11c (clone N418)	Biolegend	Cat# 117334; RRID: AB_2562415
Anti-mouse CD122 (clone TM-β1)	Miltenyi Biotec	Cat# 130-102-517; RRID: AB_2654768
Anti-mouse CD127 (clone A7R34)	Biolegend	Cat# 135010; RRID: AB_1937251, Cat# 135012: RRID: AB_1937216, Cat# 135014; RRID: AB_1937265
Anti-mouse CD137 (clone 17B5)	Biolegend	Cat# 106110; RRID: AB_2564297
Anti-mouse CD19 (clone eBio1D3)	ThermoFisher	Cat# 11-0193-82; RRID: AB_657666, Cat# 12-0193-81; RRID: AB_657661
Anti-mouse CD19 (clone 6D5)	Biolegend	Cat# 115553; RRID: AB_2564000
Anti-mouse CD244 (clone 2B4)	ThermoFisher	Cat# 17-2441-82; RRID: AB_11151150
Anti-mouse CD3e (clone 145-2C11)	ThermoFisher	Cat# 11-0031-82; RRID: AB_464882
Anti-Mouse CD3e (clone 500A2)	BD Biosciences	Cat# 560771; RRID: AB_1937314
Anti-mouse CD39 (clone Duha59)	Biolegend	Cat# 143811; RRID: AB_2750321
Anti-mouse CD4 (clone GK1.5)	Biolegend	Cat# 100414; RRID: AB_312699, Cat# 100434; RRID: AB_893324
Anti-mouse CD4 (clone RM4-4)	Biolegend	Cat# 116004; RRID: AB_313689
Anti-mouse CD4 (clone RM4-5)	Biolegend	Cat# 100526; RRID: AB_312727
Anti-mouse CD44 (clone IM7)	ThermoFisher	Cat# A25989; RRID: AB_2536050, Cat# 56-0441-82; RRID: AB_494011, Cat# A14791; RRID: AB_2534306
Anti-mouse CD45 (clone 30F-11)	Biolegend	Cat# 103107; RRID: AB_312972 Cat# 103131; RRID: AB_893344
Anti-mouse CD45.1 (clone A20)	Biolegend	Cat# 110706; RRID: AB_313495
Anti-mouse CD45.2 (clone TM)	Biolegend	Cat# 109847; RRID: AB_2616859
Anti-mouse CD5 (clone 53-7.3)	BD Biosciences	Cat# 11-0051-81; RRID: AB_464907, Cat# MA5-17784; RRID: AB_2539168, Cat# 17-0051-81; RRID: AB_469330 or Cat# 563194; RRID: AB_2738061
Anti-mouse CD62L (clone MEL-14)	ThermoFisher	Cat# 11-0621-82; RRID: AB_465109
Anti-mouse CD69 (clone H1.2F3)	Biolegend	Cat# 104536; RRID: AB_2565583

(*Continued on next page*)

Please cite this article in press as: Hanna et al., Interleukin-10 receptor signaling promotes the maintenance of a PD-1^{int} TCF-1^{+} CD8^{+} T cell population that sustains anti-tumor immunity, Immunity (2021), https://doi.org/10.1016/j.immuni.2021.11.004

Continued

REAGENT or RESOURCE	SOURCE	IDENTIFIER
Anti-mouse CD8a (clone 53-6.7)	Biolegend	Cat# 100713; RRID: AB_312752, Cat# 100743; RRID: AB_2561352
Anti-mouse CD8b (clone H35-17.2)	Miltenyi Biotec	Cat# 149031; RRID: AB_2565939, Cat# 149019; RRID: AB_ 2565702
Anti-mouse c-Jun (clone 60A8)	Cell Signaling Technology	Cat# 15683; RRID: AB_2798752
Anti-mouse CX3CR1 (clone SA011F11)	Biolegend	Cat# 149031; RRID: AB_2565939
Anti-mouse Eomes (clone Dan11-mag)	ThermoFisher	Cat# 46-4875-82; RRID: AB_10597455
Anti-mouse CD357 (GITR) (clone DTA-1)	Biolegend	Cat# 126316; RRID: AB_2563384
Anti-mouse Granzyme B (clone NGZB)	ThermoFisher	Cat# 11-8898-82; RRID: AB_10733414, Cat# 50-8898-82; RRID: AB_11219679
Anti-mouse IFNγ (clone XMG1.2)	ThermoFisher	Cat# 45-7311-80; RRID: AB_906239
Anti-mouse Ki-67 (clone SolA15)	ThermoFisher	Cat# 11-5698-82; RRID: AB_11151330
Anti-mouse KLRG1 (clone MAFA)	Biolegend	Cat# 138429; RRID: AB_2629749
Anti-mouse LAG3 (clone eBioC9B7W)	ThermoFisher	Cat# 25-2231-82; RRID: AB_257342
Anti-mouse Ly6C (clone AL-21)	BD Biosciences	Cat# 560596; RRID: AB_1727555
Anti-mouse Ly6G (clone 1A8)	BD Biosciences	Cat# 560603; RRID: AB_1727564
Anti-mouse Ly108 (clone 13G3)	BD Biosciences	Cat# 740628; RRID: AB_2740323
Anti-mouse MHC-II I-A/I-E (clone M5/ 114.15.2)	ThermoFisher	Cat# 56-5321-82; RRID: AB_494009
Anti-mouse NK1.1 (clone PK136)	Biolegend	Cat# 108714; RRID: AB_389364
Anti-mouse PD-1 (clone RMP1-30)	Biolegend	Cat# 109104; RRID: AB_313421, Cat# 109112; RRID: AB_10612938, Cat# 109116; RRID: AB_2566548
Anti-mouse PD-1 (clone 29F.1A12)	Biolegend	Cat# 135206; RRID: AB_1877231 Cat# 135228; RRID: AB_2566006
Anti-mouse PD-L1 (clone MIH5)	ThermoFisher	Cat# 46-5982-82; RRID: AB_2573819, Cat# 12-5982-82; RRID: AB_466089
Anti-mouse T-bet (clone 4B10)	Biolegend	Cat# 644828; RRID: AB_2565677
Anti-mouse TCF-1 (clone C63D9)	Cell Signaling Technologies	Cat# 6444; RRID: AB_2797627, Cat# 6709; RRID: AB_2797631
Anti-mouse TCR-beta chain (clone H57-597)	Biolegend	Cat# 109222; RRID: AB_893625
Anti-mouse TIGIT (clone Vstm3)	Biolegend	Cat# 142110; RRID: AB_2566573
Anti-mouse TIM-3 (clone RMT3-23)	ThermoFisher	Cat# 67-5870-82; RRID: AB_2744892
Anti-mouse ERK1/2 (pT202/pY204, clone 20A)	BD Biosciences	Cat# 560115; RRID: AB_399648
Anti-mouse ZAP70 (pY319)/ Syk (Y352) (clone 17A/P-ZAP70)	BD Biosciences	Cat# 561458; RRID: AB_10696417
Anti-mouse IL-10R (clone 1B1.3A)	BioXcell	Cat# BE0050; RRID: AB_1107611
rat IgG1 isotype control antibody (clone HRPN)	BioXcell	Cat# BE0088; RRID: AB_1107775
CD28 Monoclonal Antibody (clone 37.51)	ThermoFisher	Cat#: 16-0281-82; RRID AB_468921
CD3e Monoclonal Antibody (clone 145-2C11)	ThermoFisher	Cat#: 16-0031-81; RRID AB_468846
Chemicals, peptides, and recombinant proteins		
AMPure XP beads	Beckmann Coulter	Cat#: A63880
BD FACS lysing solution	BD Biosciences	Cat#: 349202
CFSE	ThermoFisher	Cat#: 65-0850-84
mouse CD90.2 microbeads	Miltenyi Biotec	Cat#: 130-049-101
eBioscience™ Foxp3 / Transcription Factor Staining Buffer Set	ThermoFisher	Cat#: 00-5523-00

(*Continued on next page*)

Please cite this article in press as: Hanna et al., Interleukin-10 receptor signaling promotes the maintenance of a PD-1^{int} TCF-1^{+} CD8^{+} T cell population that sustains anti-tumor immunity, Immunity (2021), https://doi.org/10.1016/j.immuni.2021.11.004

Continued

REAGENT or RESOURCE	SOURCE	IDENTIFIER
eBioscience™ fixable viability dye 450/506/780	ThermoFisher	Cat# 65-0863-14, 65-0866-14, 65-0865-14
IC Fixation Buffer	ThermoFisher	Cat#: 00-8222-49
eBioscience™ Protein Transport Inhibitor Cocktail (500X)	ThermoFisher	Cat#: 00-4980-03
eBioscience™ Cell Stimulation Cocktail (500X)	ThermoFisher	Cat#: 00-4970-03
Red Blood Cell Lysis Solution (10 ×)	Miltenyi Biotec	Cat#: 130-094-183
123count eBeads™ Counting Beads	ThermoFisher	Cat#: 01-1234-42
Recombinant Murine IL-10	PeproTech	Cat#: 210-10
Critical commercial assays		
EasySep™ Mouse Pan-B Cell Isolation Kit	StemCell Technologies, Inc.	Cat#: 19844
EasySep™ Mouse CD8+ T Cell Isolation Kit	StemCell Technologies, Inc.	Cat#: 19853
GentleMacs C tubes	Miltenyi Biotec	Cat#:130-093-237
RNeasy® Micro kit	QIAGEN	Cat#: 74004
RNA RNeasy mini kit	QIAGEN	Cat#: 000074104
Allprep DNA/RNA mini kit	QIAGEN	Cat#: 80204
Affymetrix GeneChip™ WT Pico Kit	Applied Biosystems (ThermoFisher)	Cat#: 902622
Affymetrix GeneChip™ Mouse Gene 2.0 ST Array	Applied Biosystems (ThermoFisher)	Cat#: 902119
Affymetrix GeneChip® Human Exon 1.0 ST Array	Applied Biosystems (ThermoFisher)	Cat#: 900651
Agilent RNA 6000 Nano Kit	Agilent	Cat#: 5067-1511
SMARTScribe reverse transcriptase	Takara	Cat#: 639537
Nextera DNA Library Preparation Kit	Illumina	Cat#: FC-121-1030
Illumina TruSeq RNA sample preparation kit v2	Illumina	Cat#: RS-122-2001
Chromuim™ Single Cell A scRNA sequencing Chip kit, 16 rxns	10x Genomics	Cat#: PN-1000009
Chromuim™ Single Cell 3′ Library & Gel Bead Kit v2, 4 rxns	10x Genomics	Cat#: PN-120267
Chromuim™ Single Cell 5′ Library & Gel Bead Kit v2, 4 rxns	10x Genomics	Cat#: PN-1000014
Chromuim™ Single Cell 3′/5′ Library Construction Kit, 16 rxns	10x Genomics	Cat#: PN-1000020
Chromuim™ Single Cell V(D)J scRNA sequencing Enrichment Kit, Mouse T cell, 96 rxns	10x Genomics	Cat#: PN-1000071
Deposited data		
RNA-seq data of T cells from 3 breast cancer patients	Gene Expression Omnibus (GEO) Azizi et al., 2018	GEO: GSE114724
Single-cell data of CD8^{+} T cells from 2 TCL1 AT mice and of PD-1^{+} CD8^{+} T cells from 1 TCL1 AT mouse	European Nucleotide Archive (ENA)	PRJEB47247 and ERP131514
Microarray data	Gene Expression Omnibus (GEO)	GEO: GSE102601 and GEO: GSE102602
Raw data fastq files of RNA-seq data of CLL patients Processed count tables of RNA seq and survival data of CLL patients	European Genome-Phenome Archive (EGA) Bioconductor package pace BloodCancerMultiOmics2017	accession EGAS0000100174
Experimental models: organisms/strains		
Mouse: C57BL/6 (WT)	Charles River Laboratories	N/A

(*Continued on next page*)

Please cite this article in press as: Hanna et al., Interleukin-10 receptor signaling promotes the maintenance of a PD-1^{int} TCF-1^{+} CD8^{+} T cell population that sustains anti-tumor immunity, Immunity (2021), https://doi.org/10.1016/j.immuni.2021.11.004

CellPress

Continued

REAGENT or RESOURCE	SOURCE	IDENTIFIER
Mouse: *Il10rb*$^{-/-}$ (*Il10rb*^{tm1Agt})	Jackson Lab Stock No: 005027	MGI: 3603437
Mouse: B6.SJL-Ptprc^{a} Pepc^{b}/BoyJ (crossed with WT C57BL/6 mice)	ZTL German Cancer Research Center (DKFZ Heidelberg)	MGI: 2164701
Mouse: *Rag2*$^{-/-}$ (*B6-Rag2*^{tm1Fwa})	ZTL German Cancer Research Center (DKFZ Heidelberg)	MGI: 1858556
Mouse: *Eμ*-TCL1 (B6-Tg(Igh-V186.2-TCL1A)3Cro)	Bichi et al., 2002	MGI: 3527221
Mouse: *Cd4*^{Cre} *x Stat3*$^{flox/flox}$ (129-*Stat3*^{tm2Aki} Tg(Lck-cre)1Jtak / Aki)	Takeda et al., 1998	N/A
Mouse: IL-10 reporter (*B6-Foxp3*^{tm1Flv} *x Il10*^{tm1Flv})	Kamanaka et al., 2006	N/A
Oligonucleotides		
Primer for TCR beta chain gene: 5′-CAATCTCTGCTTTTGATG-3′	This Paper	N/A
ATAC sequencing i7 index primers	See Table S1	N/A
Barcoded megaprimer for TCR-seq	Illumina Adapters + barcode + C-Primer	N/A
Software and algorithms		
Prism 5.04	GraphPad	https://www.graphpad.com/scientific-software/prism/
FlowJo X 10.0.7 software	FlowJo	https://www.flowjo.com/
FACSDiva Software	BD Biosciences	https://www.bdbiosciences.com/en-us/products/software/instrument-software/bd-facsdiva-software#Overview
Affymetrix Power Tools	APT	http://media.affymetrix.com/support/developer/powertools/changelog/index.html
Bioconductor annotation package TxDb.Mmusculus.UCSC.mm9.knownGene	Carlson and Maintainer, 2015	http://www.bioconductor.org/packages/release/data/annotation/html/TxDb.Mmusculus.UCSC.mm9.knownGene.html
Bioconductor: BiomaRt (v2.30.0)	Durinck et al., 2009	https://bioconductor.org/packages/release/bioc/html/biomaRt.html
Bioconductor: ChIPseeker	Yu et al., 2015	https://bioconductor.org/packages/release/bioc/html/ChIPseeker.html
Bioconductor: DiffBind	Ross-Innes et al., 2012	https://bioconductor.org/packages/release/bioc/html/DiffBind.html
Bioconductor: Limma package	Smyth, 2004	https://bioconductor.org/packages/release/bioc/html/limma.html
Bioconductor package: Pathview (v 1.14.0)	Luo and Brouwer, 2013	https://www.bioconductor.org/packages/release/bioc/html/pathview.html
Bioconductor package: DESeq2	Love et al., 2014	https://bioconductor.org/packages/release/bioc/html/DESeq2.html
Seurat	Hao et al., 2021	https://www.rdocumentation.org/packages/Seurat/versions/4.0.4
Monocle3	Cao et al., 2019	https://www.rdocumentation.org/packages/monocle3/versions/1.0.0
Bioconductor package: Nebulosa	Alquicira-Hernandez and Powell, 2021	https://github.com/powellgenomicslab/Nebulosa
mSigDb database version 6 - GSEA, pre-ranked	Subramanian et al. 2005 Liberzon et al., 2011	https://www.gsea-msigdb.org/gsea/msigdb/
MiXCR software	Bolotin et al., 2015	https://milaboratories.com/software
VDJtools	Shugay et al., 2015	https://vdjtools-doc.readthedocs.io/en/master/input.html

(*Continued on next page*)

Please cite this article in press as: Hanna et al., Interleukin-10 receptor signaling promotes the maintenance of a PD-1^{int} TCF-1^{+} CD8^{+} T cell population that sustains anti-tumor immunity, Immunity (2021), https://doi.org/10.1016/j.immuni.2021.11.004

Continued

REAGENT or RESOURCE	SOURCE	IDENTIFIER
Polyclonal-Monoclonal Diversity (PMD) package	Afzal et al., 2019	N/A
Trimmomatic version 0.36	Bolger et al., 2014	http://www.usadellab.org/cms/?page=trimmomatic
bowtie2	Langmead and Salzberg, 2012	http://bowtie-bio.sourceforge.net/bowtie2/index.shtml
rmdup of SAMtools version 1.3	Li et al., 2009	https://sourceforge.net/projects/samtools/files/samtools/1.3.1/
"annotatePeaks.pl" - HOMER software	Heinz et al., 2010	http://homer.ucsd.edu/homer/ngs/annotation.html
Ngs.plot	Shen et al., 2014	https://github.com/shenlab-sinai/ngsplot
Centipede	Pique-Regi et al., 2011	https://rajanil.github.io/msCentipede/
robust multichip average (RMA) algorithm using aroma.affymetrix	Bengtsson et al., 2008	http://www.aroma-project.org/
STAR version 2.3.0	Dobin et al., 2013	http://code.google.com/p/rna-star/
MACS2 version 2.1.1	Zhang et al., 2008	https://github.com/taoliu/MACS/
R packages: ggplot2 and Heatmap3.	Wickham et al., 2009 Zhao et al., 2014	https://cran.r-project.org/web/packages/ggplot2/index.html https://cran.r-project.org/web/packages/heatmap3/index.html
Other		
Info to clinical trial	Stilgenbauer et al., 2009	NCT00274976

RESOURCE AVAILABILITY

Lead contact

Further information and requests for resources and reagents should be directed to and will be fulfilled by the Lead Contact, Martina Seiffert (m.seiffert@dkfz.de).

Materials availability

This study did not generate new unique reagents.

Data and code availability

Microarray and ATAC-seq datasets are available on Gene Expression Omnibus (GEO) under the accession numbers GSE102601 and GSE102602.

Single-cell RNA-seq data is available on European Nucleotide Archive (ENA) under the accession numbers PRJEB47247 and ERP131514.

The code for microarray and ATAC-seq analysis is available from https://gitlab.com/dkfzmurat/il10-in-T-cells.

Raw data fastq files of RNA-seq data of CLL patients can be downloaded from European Genome-Phenome Archive (EGA), accession EGAS0000100174. Processed count tables and survival data are accessible through the Bioconductor package BloodCancerMultiOmics2017 as described previously (Dietrich et al., 2018).

EXPERIMENTAL MODEL AND SUBJECT DETAILS

Human samples

Peripheral blood (PB) and lymph node (LN) samples were obtained from CLL patients after informed consent and according to the declaration of Helsinki. All CLL cases used in this study matched the standard diagnostic criteria for CLL. Peripheral blood mononuclear cells (PBMCs) were isolated on a Ficoll density gradient (1.077 g/mL) by collecting the interphase cells after centrifugation at 1,000 g for 20 min. Primary cells from LNs were resuspended in RPMI 1640 (Life Technologies) culture medium and flushed through a fine needle to obtain single cell suspensions (Montraveta et al., 2016). Clinical information of patients is provided in Table S3.

Mice and tumor models

C57BL/6 wild-type (WT) and *Il10rb*^{tm1Agt} (*Il10rb*$^{-/-}$) mice were purchased from Charles River Laboratories (Sulzfeld, Germany) and Jackson laboratories (Bar Harbor, ME), respectively. Congenic CD45.1^{+} CD45.2^{+} and *Rag2*$^{-/-}$ mice (Shinkai et al., 1992) on C57BL/6

Please cite this article in press as: Hanna et al., Interleukin-10 receptor signaling promotes the maintenance of a PD-1^{int} TCF-1^{+} CD8^{+} T cell population that sustains anti-tumor immunity, Immunity (2021), https://doi.org/10.1016/j.immuni.2021.11.004

background were acquired from the central animal facility of the German Cancer Research Center (DKFZ Heidelberg). *Eμ*-TCL1 (TCL1) on C57BL/6 background, *Cd4*^{Cre} x *Stat3*$^{flox/flox}$ (*Stat3*$^{-/-}$) and IL-10 reporter (FIR x *tiger*) mice were previously described (Bichi et al., 2002; Kamanaka et al., 2006; Takeda et al., 1998).

Adoptive transfer of TCL1 tumors was performed as previously described (Hanna et al., 2016; McClanahan et al., 2015). Briefly, malignant B cells were enriched from splenocytes of TCL1 mice using EasySep Mouse Pan-B Cell Isolation Kit (StemCell Technologies, Inc., Cologne, Germany), or by depletion of T cells using mouse CD90.2 microbeads (Miltenyi Biotec, Bergisch Gladbach, Germany), according to the respective manufacturer's protocol. The CD5^{+}CD19^{+} content of purified cells was typically above 95%, as measured by flow cytometry. 1-4x10^{7} malignant TCL1 splenocytes were transplanted by intravenous (i.v.) or intraperitoneal (i.p.) injection into 2-3-months-old C57BL/6 WT or transgenic females. For CD8^{+} T cell transfer experiments, CD8^{+} T cells were purified from spleens of *Il10rb*$^{+/+}$, *Il10rb*$^{-/-}$, *Stat3*$^{flox/flox}$ (*Stat3*$^{+/+}$) or *Cd4*^{Cre} x *Stat3*$^{flox/flox}$ (*Stat3*$^{-/-}$) mice using EasySep Mouse CD8^{+} T Cell Isolation Kit (StemCell Technologies). *Rag2*$^{-/-}$ mice were transplanted with 5x10^{6} CD8^{+} T cells or PBS, and after 1 day, mice were transplanted with T cell depleted malignant TCL1 splenocytes. In the CD8^{+} T cell co-transfer experiment, CD8^{+} T cells from *Il10rb*$^{-/-}$ and congenic CD45.1/CD45.2 mice were mixed in 1:1 ratio. *Rag2*$^{-/-}$ mice were transplanted with 1x10^{6} mixed CD8^{+} T cells, and after 1 day, mice were transplanted with T cell depleted malignant TCL1 splenocytes.

For the CD8^{+} T cell re-transplantation experiment, splenic PD-1^{+} CD8^{+} T cells were isolated from leukemic WT and *IL10rb*$^{-/-}$ mice and transplanted into *Rag2*$^{-/-}$ mice prior tumor cell injection. More specifically, splenocytes from leukemic WT and *IL10rb*$^{-/-}$ mice were enriched for CD8^{+} T cells using the EasySep Mouse CD8^{+} T Cell Isolation Kit (StemCell Technologies). Next, DAPI^{-}/Lin^{-}/TCRb^{+}/CD8^{+}/PD-1^{+} cells were = sorted by flow cytometry, and 5x10^{4} PD-1^{+} CD8^{+} T cells from either leukemic WT or leukemic *IL10rb*$^{-/-}$ mice were i.v. injected into 7-week-old *Rag2*$^{-/-}$ mice. Sorted PD-1^{+} CD8^{+} T cells from one donor mouse were injected into one or two *Rag2*$^{-/-}$ mice, depending on the number of sorted PD-1^{+} CD8^{+} T cells. One day after T cell injection, 5x10^{5} malignant TCL1 cells were i.v. injected into *Rag2*$^{-/-}$ mice. Prior to malignant cell transplantation, splenocytes from leukemic TCL1 AT mice were enriched for B cells by negative depletion of unwanted cells using the Easysep Mouse Pan-B Cell Isolation Kit according to manufacturer's instructions. Tumor progression was monitored in PB and mice were sacrificed 5.5 weeks after malignant cell injection. Spleens were dissected and tumor load was analyzed.

All animal experiments were carried out according to governmental and institutional guidelines and authorized by the local authorities (Regierungspräsidium Karlsruhe, permit numbers: G-36/14, G-123/14, G-16/15, G-53/15, and G-98/16).

METHOD DETAILS

Antibody treatment

For IL-10R blockade experiments, mice were first transplanted with TCL1 leukemia cells. After 3 weeks, mice were assigned to different treatment arms according to the percentage of CD5^{+}CD19^{+} (CLL) cells out of CD45^{+} cells in PB. Subsequently, mice were injected i.p. with 1 mg of αIL-10R (clone: 1B1.3A) or rat IgG1 isotype control antibody (clone: HRPN), followed by subsequent doses of 0.5 mg every 3 days for another 2 weeks. All antibodies for *in vivo* experiments were acquired from BioXcell (West Lebanon, NH).

Collection of tissue samples and preparation of cell suspensions

Mice were euthanized by increasing concentrations of carbon dioxide (CO_2). PB was drawn from the submandibular vein or via cardiac puncture and collected in ethylenediaminetetraacetic acid (EDTA)-coated tubes (Sarstedt, Nümbrecht, Germany). Single-cell suspensions from spleens, bone marrow (BM) and inguinal LNs were prepared as previously described (Hanna et al., 2016; McClanahan et al., 2015). BM cells were flushed from femurs with 5 mL of phosphate-buffered saline (PBS)/5% fetal calf serum (FCS). Spleen single-cell suspensions were generated by using the gentleMACS tissue dissociator with Gentle MACS tubes C (Miltenyi Biotec). Single cell suspensions from LNs were prepared by grinding the tissue through 70 μm cell strainers (BD Biosciences, Heidelberg, Germany). Erythrocytes were lysed by using Red blood cell lysis buffer (Mitenyi Biotec).

Flow cytometry

After preparations of single-cell suspensions, cells were incubated with recommended dilutions of antibodies against cell surface proteins in PBS containing 0.1% fixable viability dye (eBioscience, Frankfurt am Main, Germany) for 30 min at 4°C. Cells were fixed using IC fixation buffer (eBioscience), washed and stored at 4°C in the dark until analyzed by flow cytometry.

For transcription factor and IL-10 intracellular staining, cells were fixed after surface molecule staining with Foxp3 fixation/permeabilization buffer (eBioscience) for 30 min at room temperature, followed by permeabilization with 1X permeabilization buffer (eBioscience) and then staining with antibodies against transcription factors in 1X permeabilization buffer for 30 min at room temperature. After washing twice with 1X permeabilization buffer, cells were resuspended in a final volume of 200 μl 1X permeabilization buffer and stored at 4°C in the dark until analyzed by flow cytometry.

For labeling of cells in whole blood, 50-100 μl of PB were stained with antibodies specific for surface molecules for 30 min at 4°C, followed by incubation for 10 min with 2 mL of 1x BD FACS lysing solution (BD Biosciences) to remove erythrocytes. After centrifugation, supernatants were carefully aspirated, and pelleted cells were resuspended in 150 μl of 1x BD FACSLysing solution. 50 μl of 123count eBeads (eBioscience) were directly added before data acquisition. Absolute cell numbers in blood were calculated according to the formula: absolute count (cells/μL) = (cell count **x** bead volume x bead concentration)/ (bead Count **x** cell Volume).

Please cite this article in press as: Hanna et al., Interleukin-10 receptor signaling promotes the maintenance of a PD-1^{int} TCF-1^{+} CD8^{+} T cell population that sustains anti-tumor immunity, Immunity (2021), https://doi.org/10.1016/j.immuni.2021.11.004

For all flow cytometric measurement, data acquisition was done using BD LSRII or BD FACSCanto flow cytometer (BD Biosciences). Median Fluorescence Intensity (MFI) was recorded and normalized by subtracting the MFI of the respective fluorescence-minus-one (FMO) control. Data analysis was performed using FlowJo X 10.0.7 software (FlowJo, Ashland, OR, USA). Gating strategies are depicted in the supplementary information.

For cell sorting, splenocytes were enriched for CD8^{+} T cells using EasySep Mouse CD8^{+} T Cell Isolation Kit (Stem Cell Technologies). Cells were stained for cell surface proteins. CD8^{+} T cells were defined as DAPI^{-} Lin^{-} (CD19^{-} CD11b^{-} NK1.1^{-}) TCRb^{+} CD8^{+}, and different T cell subsets were sorted in PBS with 5% FCS using BD FACSAria II (BD Biosciences) running with FACSDiva Software (BD Biosciences). Purity of sorted cells was typically above 95%.

Analysis of functional capacity of CD8^{+} T cells ex vivo

Cytokine release, granzyme B production and degranulation capacity of CD8^{+} T cells were assayed, as previously described (Hanna et al., 2019; McClanahan et al., 2015). Cells were resuspended in complete medium (DMEM supplemented with 10% FSC, 10 mM HEPES, 1 mM sodium pyruvate, 0.1% β-mercaptoethanol, 100 U/mL penicillin, and 100 μg/mL streptomycin), and seeded at a density of 3x10^{6} cells/ 200 μl. Cells were incubated in cell stimulation cocktail in the presence of protein transport inhibitor cocktail (both from eBioscience) for 6 h at 37°C/ 5% CO_2. Degranulation capacity of T cells was measured by adding fluorochrome-conjugated CD107a antibody (eBioscience) to the culture, as previously described (Betts et al., 2003). Afterward, cells were washed, stained for surface proteins and fixed using IC fixation buffer (eBioscience). After washing with 1X permeabilization buffer, cells were stained with fluorescently labeled antibodies against intracellular proteins for 30 min at room temperature in the dark, washed and analyzed by flow cytometry.

CD8^{+} T cell:CLL cell conjugation and immunological synapse assays

Immune cells were isolated from splenocytes of leukemic *Rag2*$^{-/-}$ mice, previously injected with *IL10rb*$^{-/-}$ or WT CD8^{+} T cells and CD5^{+} CD19^{+} TCL1 tumor cells. Purified B cells (CD19^{+} negative magnetic isolation) were stained with CMAC blue (ThermoFisher Scientific), following the manufacturer's instructions and pulsed with 2 μg/mL of staphylococcal superantigens (sAgs; SEA and SEB; Sigma-Aldrich) for 30 min at 37°C. Purified T cells (negative magnetic isolation) were pooled with target B cells at equal numbers (5x10^{5} cells), centrifuged at 250 g for 5 min, and incubated at 37°C for further 10 min. Cell conjugates were transferred onto poly-L-lysine-coated slides (ThermoFisher Scientific) using a cell concentrator (Cytofuge 2) and fixed for 15 min at room temperature with 3% methanol-free formaldehyde (ThermoFisher Scientific) in PBS, permeabilized with 0.3% Triton X-100 (Sigma-Aldrich) in PBS for 5 min and incubated for 10 min with 5% donkey serum (Sigma-Aldrich) in PBS (blocking solution). Primary (anti-mouse granzyme B, Cell Signaling) and secondary antibodies (donkey anti-rabbit Alexa Fluor 647) were applied sequentially for 45 min at 4°C in 5% goat serum in PBS. F-actin was stained with rhodamine-phalloidin (ThermoFisher Scientific) following the manufacturer's instructions. After washing, slides were sealed with coverslips using mounting solution (FluorSaveTM reagent; Merck Millipore). The specificity of staining was optimized and controlled by using appropriate dilutions of isotype-control, primary antibodies and subsequent fluorescent secondary antibodies. Background staining using antibodies alone was compared with positively stained cells and was not visible when using identical acquisition settings. Medial optical section images (or Z stacks for 3D volume images) were captured with a high-sensitivity A1R confocal microscope (with gallium arsenide phosphide, GaAsP detector) using a 63X/1.40 oil objective with NIS-elements imaging software (Nikon). Detectors were set to detect an optimal signal below saturation limits. Fluorescence was acquired sequentially to prevent passage of fluorescence from other channels (DU4 sequential acquisition). Image sets to be compared were acquired during the same session using identical acquisition settings. Blinded confocal images were analyzed using NIS-Elements image analysis software (Nikon). CD8^{+} T cell:CLL cell conjugates were identified only when CD8^{+} cells (F-actin staining only) were in direct contact interaction with target CLL cells (blue fluorescent channel). For % conjugated T cell analysis, all T cells were scored per sample image for the number of F-actin (red)$^{+}$ T cells forming conjugates with CLL cells (CMAC blue) and the percentage calculated (n = 8 images per sample). To measure CD8^{+} T cell immune synapse formation (area), the Region of Interest (ROIs) analysis tool was used to measure the total area (μm^{2}) of F-actin (n = 50 T cell conjugates per sample) or mean fluorescence intensity (MFI) of granzyme B (n = 30 T cell conjugates per sample) accumulated at all CD8^{+} T cell contact sites and immune synapses with target tumor CLL cells. Data were analyzed using GraphPad Prism software.

Analysis of TCR activity and T cell proliferation of CD8^{+} T cells ex vivo

CD8^{+} T cells from splenocytes of C57BL/6 mice were isolated using EasySep Mouse CD8^{+} T Cell Isolation Kit (StemCell Technologies). 2x10^{4} cells were seeded in αCD3-coated wells (1 μg/mL) and cultured for 2-3 days in the presence of recombinant IL-10 (150 U/mL). Consequently, cells were harvested and stained for flow cytometry analysis. For proliferation assessment, CD8^{+} T cells were labeled with CFSE (5 μM) prior seeding, and CFSE dilution was analyzed by flow cytometry. For measurement of pZAP70 and pERK1/2 proteins, cultured CD8^{+} T cells were re-stimulated with αCD3 (10 μg/mL) for 1, 2, 5, 10 and 30 min prior direct cell fixation and analysis by flow cytometry.

Microarray data analysis of CD8^{+} T cells

Total ribonucleic acid (RNA) was extracted from sorted cells using the RNeasy® Micro kit (QIAGEN, Hilden, Germany) according to manufacturer's protocol. The laboratory work was done in the Genomics and Proteomics Core Facility at the German Cancer Research Center, Heidelberg, Germany (DKFZ). Biotin-labeled ss-cDNA samples for hybridization on GeneChip Mouse Gene

Please cite this article in press as: Hanna et al., Interleukin-10 receptor signaling promotes the maintenance of a PD-1^{int} TCF-1^{+} CD8^{+} T cell population that sustains anti-tumor immunity, Immunity (2021), https://doi.org/10.1016/j.immuni.2021.11.004

2.0 ST Arrays (Affymetrix) were prepared according to Affymetrix's recommended sample labeling procedure as described in the Gene Chip WT Pico Reagent Kit guide. In brief, 500 pg total RNA was used for complementary DNA (cDNA) synthesis, followed by a low cycle PCR amplification and *in vitro* transcription step to synthesize cRNA according to the Affymetrix® GeneChip® WT Pico Reagent Kit. Quality of cRNA was controlled using the RNA Nano Chip Assay on an Agilent 2100 Bioanalyzer and spectrophotometrically quantified (NanoDrop). 20 μg of cRNA was then converted to sense-strand DNA (ss-cDNA). After fragmentation and terminal labeling, 5.5 μg of biotinylated ss-cDNA were hybridized for 17 h at 45°C on Affymetrix Mouse Gene 2.0 ST Arrays. Microarray scanning was done using an Affymetrix GeneChip® Scanner 3000 according to GeneChip® Expression Wash, Stain and Scan Manual for Cartridge Arrays. Two microarray datasets were generated for i) CD8^{+} T cell subtypes (naive, memory, PD-1^{int} and PD-1^{hi} effector), and ii) αIL10R treatment of PD-1^{hi} effector CD8^{+} T cells. Both datasets were independently processed with Affymetrix Power Tools (APT, http://media.affymetrix.com/support/developer/powertools/changelog/index.html) using Robust Microarray Analysis (RMA) approach for the normalization (Irizarry et al., 2003). Log2-transformed transcript-level gene expression was calculated for 'meta' probe sets. Quality control (QC) of the samples was carried out by examining 'average raw intensity signal' ('pm_mean') or 'mean absolute deviation of the residuals' ('all_probeset_mad_residual_mean'). As similarly described in Lockstone (2011), 'detected above background' (DABG) measure was used to filter 'meta' probe sets if called as 'detected' (P value < 0.05) in at least 50% of the samples in any of the experimental groups. For the two microarray datasets of CD8^{+} T cell subtypes and αIL10R treatment, 32,114 and 30,267 'meta' probe sets were retained out of 33,793 main 'meta' probe sets (linked with 20,263 Entrez genes), respectively. Hierarchical clustering was applied in an unsupervised fashion (Pearson's correlation coefficient, average-linkage) to assess whether replicates of the same experimental groups cluster together. From the microarray dataset of αIL10R treatment, the sample 'PD-1^{hi} isotype rep1' was identified as an outlier by considering the QC metrics (e.g., 'pm_mean', 'all_probeset_mad_residual_mean') together with the unsupervised clustering. The sample 'PD-1^{hi} isotype rep1' was removed from further analysis. Limma package (Smyth, 2004) (v3.30.13, from Bioconductor) (Gentleman et al., 2004) facilitated the analysis of differential expression between the comparisons of i) CD8^{+} T cell subtypes (PD-1^{hi} versus PD-1^{int}) and ii) PD-1^{hi} αIL10R treatment versus PD-1^{hi} isotype (FDR adjusted P value < 0.05 and absolute fold change > 0.5). Functional enrichment analysis was carried out on the fold change ranked list of genes using 'Gene set enrichment analysis' (GSEA, pre-ranked) (Subramanian et al., 2005) with the latest mSigDb database version 6 (Liberzon et al., 2011). GSEA was limited to 'meta' probe sets associated with a gene symbol. Human orthologs of the 'meta' probe sets were retrieved from Ensembl (Yates et al., 2016) using R package BiomaRt (v2.30.0) (Durinck et al., 2009). In case of multiple probe sets per gene, the 'meta' probe set with the highest variance was kept for genes represented by multiple probe sets. Visualization of the cell cycle from KEGG pathways (Kanehisa and Goto, 2000) was accomplished with R package: Pathview (v 1.14.0) (Luo and Brouwer, 2013).

Single-cell RNA-seq of CD3^{+} T cells and PD-1^{+} CD8^{+} T cells from splenocytes of TCL1 AT mouse model

Three TCL1 AT mouse spleen samples were processed for scRNA-seq. CD3^{+} T cells from two samples were defined as DAPI^{-} CD45^{+} CD19^{-} CD3^{+} and sorted by flow cytometry. scRNA-seq and TCR-seq libraries were generated using the Chromium Next GEM Single Cell V(D)J Solution (v1.1 Chemistry) from 10x Genomics following the manufacturer's instructions. GEX libraries were sequenced on a NovaSeq 6000 machine (Illumina), and V(D)J-enriched libraries were sequenced on a NextSeq 550 (Illumina).

CD8^{+} PD-1^{+} T cells from one murine sample were defined as DAPI^{-} Lin^{-} (CD19^{-} CD11b^{-} NK1.1^{-}) TCRb^{+} CD8^{+} PD-1^{+} and sorted by flow cytometry. A scRNA-seq library was constructed using the 10x Genomics Single-Cell 3′ Gel Bead and Library V2 kit and sequenced on a HiSeq 4000 machine (Illumina).

Single-cell RNA-seq data processing and analysis

Raw reads in fastq format were aligned to the mm10 mouse reference genome using the Cell Ranger pipeline (10x Genomics). Sparse count matrices for each sample were generated as output files. For data normalization, scaling and dimensionality reduction and cell clustering, the Seurat v4 toolkit was used (Butler et al., 2018; Stuart et al., 2019). Cells with low-quality data were removed based on the number of genes expressed and mitochondrial gene content: cells with < 200 genes and potential doublets with > 3,000 genes, as well as cells with > 10% mitochondrial genes were removed. In addition, genes present in < 2 cells were excluded for downstream analysis. Hereafter, the two mouse datasets were analyzed using a similar workflow. Each dataset was transformed and normalized utilizing SCTransform. Per default the 3,000 most variable genes from each sample were identified for principal component (PC) analysis via RunPCA function. Sixteen PCs were considered for further cell clustering. Using the FindNeighbors function, a shared nearest neighbor graph (SNN) was created, and a hierarchical clustering using Louvain algorithm was generated with the resolution parameter set to 0.5-0.7. Non-linear dimensional reduction using UMAP was performed in order to visualize the datasets. Finally, FindAllMarkers function using the non-parametric Wilcoxon rank sum test identified differentially expressed genes for each cluster, with an adjusted (Bonferroni correction) *p*-value of 0.05 set for considering significance.

Computational separation of CD3^{+} T cells into CD8^{+} and CD4^{+} cells

Computational separation of CD8^{+} and CD4^{+} T cells was carried out in order to perform a re-clustering on only CD8^{+} T cells. Cell separation was based on a calculation of pairwise distances between gene counts and centroids of the 3,000 most variable genes between CD4^{+} and CD8^{+} specific clusters.

Please cite this article in press as: Hanna et al., Interleukin-10 receptor signaling promotes the maintenance of a PD-1^{int} TCF-1^{+} CD8^{+} T cell population that sustains anti-tumor immunity, Immunity (2021), https://doi.org/10.1016/j.immuni.2021.11.004

V(D)J T cell analysis

V(D)J transcripts from single cells were aligned and counted using the CellRanger pipeline. Non-productive, as well as productive rearrangements were evaluated. Two or more cells containing the same α- and β-chain CDR3 consensus nucleotide sequences were considered as expanded cell clones. The Seurat workflow was used for the mapping of the TCR information into the single-cell UMAP.

Single-cell trajectory analysis

Single-cell trajectory analysis was inferred using the Monocle 3 software (Qiu et al., 2017). The Seurat object created for previous analysis was converted to monocle 3 object using seurat-wrappers. Pseudotime inference was performed on the UMAP created previously by Seurat using the learn_graph function. The node within the PD-1^{lo} TCF-1^{hi} cell cluster in the trajectory was selected as the root node and visualized as a pseudotime trajectory on the UMAP.

Single-cell RNA-seq analysis of breast cancer samples

Single-cell RNA-seq data of T cells from 3 breast cancer patients was retrieved from GEO database (accession number: GSE114724) (Azizi et al., 2018). Data analysis was done using Seurat package in R (Butler et al., 2018). Patient samples were analyzed independently to avoid batch effects. Gene count tables were generated using Read10X followed by CreateSeuratObject function with logarithmic normalization of the data. To remove doublets, we excluded cells with high UMI counts (more than 15,000-20,000 UMIs based on the sample). Dimensionality reduction and clustering was performed on variable genes defined using the FindVariableGenes function in Seurat. After performing principal component analysis using RunPCA function, cell clustering was done using FindClusters followed by creating t-stochastic neighborhood embedding (tSNE) for data visualization using RunTSNE function. We then focused our analysis on CD8^{+} T cells, thus we removed clusters with high expression of *CD4* or *FOXP3,* or low expression of *CD8A.* Steps of normalizing the data, selecting variable genes, performing PCA, and creating a tSNE were repeated as before. Average expression of gene signatures per cell was calculated and plotted using the DotPlot function of the Seurat package.

Bulk TCR-sequencing

Total RNA isolated from T cell subsets was used for TCR sequencing by RACE PCR, as previously described with minor modifications (Ruggiero et al., 2015). Briefly, RNA quality was assessed with the Agilent Bioanalyzer. RACE PCR was performed on up to 250 ng RNA by first strand cDNA synthesis using the SMARTScribe reverse transcriptase (Takara). Therefore, RNA was preincubated with a primer annealing to the constant region of the TCR beta chain gene (5′- CAATCTCTGCTTTTGATG-3′) at 72°C for 4 min and at 42°C for 2 min followed by incubation at 42°C for 60 min in presence of a template-switch oligo containing a 12 bp sample specific barcode. Two nested exponential PCRs were subsequently performed using 5 μL of the single-stranded cDNA or 2 μL of the first exponential PCR product, respectively. During second exponential PCR, barcoded megaprimers were used to create libraries suitable for MiSeq sequencing. Libraries were purified with 0.65x Ampure XP beads (Beckman Coulter) and pooled for multiplex paired-end sequencing (R1 = 450 bp; R2 = 50 bp) on the MiSeq platform (Illumina).

Raw sequence reads were sorted according to their barcodes and TCR clonotypes were extracted from deep sequencing data by MiXCR software (Bolotin et al., 2015). Resulting clonotypes were filtered for nonfunctional sequences and replicates were pooled using VDJtools (Shugay et al., 2015). Shannon diversity indices (Shannon, 1997) were calculated using Polyclonal-Monoclonal Diversity (PMD) package (Afzal et al., 2019).

ATAC-seq library construction

Sorted T cell populations were incubated for 30 min at 37°C with 2.5 μl Tn5 transposase and 12.5 μl TD buffer (Nextera DNA Library Preparation Kit; Illumina) in the presence of 0.125% Igepal CA-630 (Sigma-Aldrich) in a volume of 20 μl. The reaction was stopped with EDTA (final conc. 9 mM; Invitrogen) on ice for 5 min. Barcodes were added by 13-14 PCR cycles conducted with the previously described PCR conditions (Buenrostro et al., 2013) in the presence of 1x NEBNext High-Fidelity 2X PCR Master Mix (New England Biolabs) and custom Nextera i5 and i7 index primers (Table S4) in a final concentration of 0.5 μM, before ATAC-seq libraries were purified with 1.4x Ampure XP beads (Beckman Coulter) and sequenced 100 bp paired-end on Illumina HiSeq 4000.

ATAC-seq data analysis

Sequenced ATAC-seq reads were trimmed using Trimmomatic version 0.36 to remove adaptor sequences.(Bolger et al., 2014) Trimmed reads were mapped to the mouse genome (mm9) with bowtie2 using the options ‘‘–very- sensitive -X 2000.’’(Langmead and Salzberg, 2012). Reads overlapping regions contained in the ENCODE blacklist (https://sites.google.com/site/anshulkundaje/projects/blacklists) and reads mapping to the mitochondrial genome were discarded. All reads from duplicated fragments were removed with rmdup of SAMtools version 1.3 (Li et al., 2009). Peaks were called using MACS2 version 2.1.1 (Zhang et al., 2008) with the parameters ‘‘–nomodel -shift −10–extsize 28–broad.’’ To represent the 29 bp region originally occupied by the Tn5 transposase (Adey et al., 2010), all ATAC-seq reads were shifted to be positioned at the cutting site of the Tn5 transposase for all downstream analysis. R package, DiffBind (Ross-Innes et al., 2012) was employed to quantify ATAC-seq signal for MACS-called peaks and to identify differentially accessible sites between αIL10R-treated and untreated PD-1^{hi} effector CD8^{+} T cells with the default method of DESeq2 (Love et al., 2014). ATAC-seq peaks were annotated with the annotatePeak function from the R package ChIPseeker (Yu et al., 2015) by setting the transcriptional start site region from −1500 to 1500 and using the Bioconductor annotation

package TxDb.Mmusculus.UCSC.mm9.knownGene (Carlson and Maintainer, 2015). Plots were generated using ggplot2 (Wickham et al., 2009) and Heatmap3 (Zhao et al., 2014) R packages.

ATAC-seq footprinting

Sequencing reads of same subpopulations from different individuals were combined for the footprinting analysis and collapsed to the base of the original position of the transposase. Genomic location of motifs which were found to be enriched in peaks with differential ATAC-seq signal were identified with ''annotatePeaks.pl'' of the HOMER software in the corresponding peak set (Heinz et al., 2010). Ngs.plot (Shen et al., 2014) was used to obtain normalized read coverage over 100 bins and to generate average profile plots for indicated regions around the center of the motif. Normalized reads generated by ngs.plot were multiplied by 500 for better visualization in heatmap and ordered according to the posterior probability score calculated by Centipede from the ATAC-seq reads, the motif conservation score from HOMER and the PWM score (Pique-Regi et al., 2011).

Correlation of IL-10 expression with patient outcome

IL10 gene expression was derived from RNA-seq data of 123 untreated CLL patients (Dietrich et al., 2018). Briefly, RNA from CLL cells was extracted using the RNeasy mini kit (QIAGEN) according to the manufacturer's protocol. RNA quantification was performed on a Qubit 2.0 Flourometer. Quality was assessed on an Agilent 2100 Bioanalyzer. An RNA integrity number (RIN) of at least 8 was required. RNA-seq libraries were prepared according to the manufacturer's protocol (Illumina TruSeq RNA sample preparation v2). Sequencing was performed on Illumina HiSeq 2000 machines with 2–3 samples multiplexed per lane. The RNA-seq reads were demultiplexed and aligned to the human reference genome (GRCh 37.1 / hg 19) using STAR version 2.3.0 (Dobin et al., 2013) with default parameters. Read counts per gene were obtained with htseq-count using the default mode union. Differential expression calling was performed using DESeq2 (Love et al., 2014). Cox regression modeling was performed to assess the impact of *IL10* mRNA expression on time to next treatment which was dichotomized at median expression of *IL10* and plotted using the Kaplan-Meier method.

In an independent cohort of 73 relapsed/refractory CLL patients, *IL10* transcript expression was derived from a gene expression profiling series conducted on PBMCs from patients enrolled on a multicenter phase 2 trial (NCT00274976) (Stilgenbauer et al., 2009). Specimen were collected at enrolment on the trial and before application of therapy. Ficoll density gradient (1.077 g/mL) centrifugation at 1,000 g for 20 min was used to select PBMCs. Extraction of mRNA for expression profiling was done by using the Allprep DNA/RNA mini kit (QIAGEN). Quality control on purity, concentration and RNA integrity was performed using the Agilent 2100 Bioanalyzer with the RNA 6000 Nano LabChip (Agilent Technologies) and the 2100 Expert Software. Specimen used for gene expression profiling had an RIN of at least 7.0. Expression profiling was conducted on the Affymetrix GeneChip® Human Exon 1.0 ST Array (Affymetrix, Santa Clara, CA, USA). According to the manufacturer's protocol instructions, 250 ng RNA per specimen were amplified, transcribed to cDNA, fragmented and subsequently labeled with Biotin. Array hybridization in the Affymetrix GeneChip® Hybridization Oven 640 was performed at 45°C for 16-18 h, arrays were subsequently washed in the Fluidics Station 450 and scanned on the GeneChip scanner 3000 7G. Raw Affymetrix Human Exon array data files have been preprocessed by the robust multichip average (RMA) algorithm using aroma.affymetrix. Gene expression values were summarized on the transcript level using the 'core' probe set definition according to Affymetrix (Bengtsson et al., 2008). Progression-free survival (PFS) and overall survival (OS) was compared for patients with high and low *IL10* expression, dichotomized at median expression of *IL10*.

QUANTIFICATION AND STATISTICAL ANALYSIS

Statistical analysis

Data were analyzed using Prism 5.04 GraphPad software. Comparisons of two different sample groups were performed using unpaired t test with Welch approximation to account for unequal variances, unless otherwise indicated. Paired t test was used when comparing two cell populations within the same sample. One-way ANOVA analysis followed by Tukey's multiple comparison test or Kruskal-Wallis test were used for multiple group comparisons. Correlation between two parameters was calculated using Spearman's rank correlation coefficient. Values of $p < 0.05$ were considered to be statistically significant. All graphs show means ± SEM, unless otherwise indicated.